JOINT TRANSPORTATION
RESEARCH PROGRAM
INDIANA DEPARTMENT OF TRANSPORTATION
AND PURDUE UNIVERSITY

Experimental Study of the Load Response of Large Diameter Closed-Ended and Open-Ended Pipe Piles Installed in Alluvial Soil

Fei Han, Eshan Ganju, Rodrigo Salgado,
Monica Prezzi, Mir Zaheer

SPR-4040 • Report Number: FHWA/IN/JTRP-2019/03 • DOI: 10.5703/1288284316880

RECOMMENDED CITATION

Han, F., Ganju, E., Salgado, R., Prezzi, M., & Zaheer, M. (2019). *Experimental study of the load response of large diameter closed-ended and open-ended pipe piles installed in alluvial soil* (Joint Transportation Research Program Publication No. FHWA/IN/JTRP-2019/03). West Lafayette, IN: Purdue University. https://doi.org/10.5703/1288284316880

AUTHORS

Fei Han
Eshan Ganju
Graduate Research Assistants
Lyles School of Civil Engineering
Purdue University

Rodrigo Salgado, PhD
Charles Pankow Professor of Civil Engineering
Lyles School of Civil Engineering
Purdue University
(765) 494-5030
rodrigo@ecn.purdue.edu
Corresponding Author

Monica Prezzi, PhD
Professor of Civil Engineering
Lyles School of Civil Engineering
Purdue University

Mir Zaheer, PE
Geotechnical Design Engineer
Indiana Department of Transportation

JOINT TRANSPORTATION RESEARCH PROGRAM

The Joint Transportation Research Program serves as a vehicle for INDOT collaboration with higher education institutions and industry in Indiana to facilitate innovation that results in continuous improvement in the planning, design, construction, operation, management and economic efficiency of the Indiana transportation infrastructure. https://engineering.purdue.edu/JTRP/index_html

Published reports of the Joint Transportation Research Program are available at http://docs.lib.purdue.edu/jtrp/.

NOTICE

The contents of this report reflect the views of the authors, who are responsible for the facts and the accuracy of the data presented herein. The contents do not necessarily reflect the official views and policies of the Indiana Department of Transportation or the Federal Highway Administration. The report does not constitute a standard, specification or regulation.

TECHNICAL REPORT DOCUMENTATION PAGE

1. Report No. FHWA/IN/JTRP-2019/03	**2. Government Accession No.**	**3. Recipient's Catalog No.**
4. Title and Subtitle Experimental Study of the Load Response of Large Diameter Closed-Ended and Open-Ended Pipe Piles Installed in Alluvial Soil		**5. Report Date** January 2019 **6. Performing Organization Code**
7. Author(s) Fei Han, Eshan Ganju, Rodrigo Salgado, Monica Prezzi, Mir Zaheer		**8. Performing Organization Report No.** FHWA/IN/JTRP-2019/03
9. Performing Organization Name and Address Joint Transportation Research Program Hall for Discovery and Learning Research (DLR), Suite 204 207 S. Martin Jischke Drive West Lafayette, IN 47907		**10. Work Unit No.** **11. Contract or Grant No.** SPR-4040
12. Sponsoring Agency Name and Address Indiana Department of Transportation (SPR) State Office Building 100 North Senate Avenue Indianapolis, IN 46204		**13. Type of Report and Period Covered** Final Report **14. Sponsoring Agency Code**

15. Supplementary Notes

Conducted in cooperation with the U.S. Department of Transportation, Federal Highway Administration.

16. Abstract

A seven-span concrete bridge was constructed over the Wabash River in Lafayette, Indiana. The bridge, which has a total length of 305 m (1,000 ft) and typical spans of 46 m (152 ft), consists of six hammerhead bridge piers in the center and two end bents supported on open-ended and closed-ended pipe piles, respectively. According to the structural bridge design, the dead load carried by each pile ranges from 1,014 kN (228 kips) to 1,495 kN (336 kips), whereas the live load ranges from 512 kN (115 kips) to 1,188 kN (267 kips), depending on the location of the piles. A closed-ended and an open-ended test piles (with the same, or almost the same diameter for the production pile) were instrumented at the Bowen Laboratory, transported to the construction site, then driven into the ground, and statically load tested. The report presents in detail the results of the site investigation, pile instrumentation procedure, pile driving records and interpretations of the static load test results.

17. Key Words pile load test, gravel, bridge, foundation design, pile instrumentation	**18. Distribution Statement** No restrictions. This document is available through the National Technical Information Service, Springfield, VA 22161.

19. Security Classif. (of this report) Unclassified	**20. Security Classif. (of this page)** Unclassified	**21. No. of Pages** 42	**22. Price**

Form DOT F 1700.7 (8-72) Reproduction of completed page authorized

EXECUTIVE SUMMARY

EXPERIMENTAL STUDY OF THE LOAD RESPONSE OF LARGE DIAMETER CLOSED-ENDED AND OPEN-ENDED PIPE PILES INSTALLED IN ALLUVIAL SOIL

Introduction

A seven-span concrete bridge was constructed over the Wabash River in Lafayette, Indiana. The bridge, which has a total length of 305 m (1,000 ft) and typical spans of 46 m (152 ft), consists of six hammerhead bridge piers in the center and two end bents supported on open-ended and closed-ended pipe piles, respectively. According to the structural bridge design, the dead load carried by each pile ranges from 1,014 kN (228 kips) to 1,495 kN (336 kips), whereas the live load ranges from 512 kN (115 kips) to 1,188 kN (267 kips), depending on the location of the piles. A closed-ended and an open-ended test pile (with the same, or almost the same, diameter for the production pile) were instrumented at the Bowen Laboratory, transported to the construction site, then driven into the ground and statically load tested. This report presents in detail the results of the site investigation, pile instrumentation procedure, pile driving records, and interpretations of the static load test results.

Findings

The driving resistance (blow counts) for the closed-ended pile was consistently greater than that of the open-ended pipe at any given depth. The final plug length ratio (PLR) for the open-ended test pile was 77.7% at the end of driving. Based on the static load tests, the ultimate resistances were 4,559 kN (1,025 kips) for the closed-ended test pile and 4,782 kN (1,075 kips) for the open-ended test pile. The open-ended pile showed greater additional resistance mobilization from the ultimate load to the plunging load than did the closed-ended pile; this is due to the contribution from the plug to the total pile resistance.

Representative CPT-based pile design methods were used for the estimation of the bearing capacity of the test piles. The design methods provide good estimates for the shaft resistance in sandy soil with low gravel content ($<20\%$) but significantly overpredict the shaft resistance in soil with a high gravel content ($>30\%$). The base resistance was significantly overestimated for the closed-ended pile due to the high gravel content (near 50%) found at the depth of the pile base. In contrast, a good estimate was found for the base resistance of the open-ended pile, although its pile base was also located in soil with a high gravel content. The reason for this is that the annulus resistance, which takes the main portion (87.6%) of the base resistance, is well represented by the cone resistance because the cone diameter is comparable to the annulus thickness.

Implementation

The unit shaft and base resistances measured from the static load tests provide a valuable reference for the design of the production piles used to support the piers and bents of the Sagamore Parkway Bridge. The study significantly advanced the understanding of the behavior of closed-ended and open-ended pipe piles driven in gravelly sand, and it brought insights into the applicability of the current CPT-based design methods for large diameter open-ended and closed-ended pipe piles in gravelly soil profiles.

CONTENTS

LIST OF TABLES

LIST OF FIGURES

1. INTRODUCTION

1.1 Background

For the first time, INDOT was using large-diameter (24 inch) closed-ended and open-ended piles to support the piers and bents of the Sagamore Parkway over the Wabash River. Preliminary site investigation results indicated that the soil profile at the construction site consists of mainly sandy soils with various gravel contents (as high as 40%–60% at certain depths). Currently, there is no established pile design method that accounts for the presence of high gravel contents in soil profile. Therefore, static load tests were performed at the construction site on densely instrumented closed-ended and open-ended test piles with dimensions that resemble those of the production piles. A double-wall instrumentation was implemented for the open-ended test pile such that measurements of the pile's inner and outer shaft resistances could be separated. The detailed resistance measurements obtained from the static load tests provide valuable guidance in the design of the production piles. The tremendous challenges present in the pile instrumentation, assembly of the double-wall system, and operation logistics for test piles of such large scale (2 ft in diameter, 60 ft and 100 ft in length) made the present side-by-side static pile load tests a unique case study in the pile testing history.

1.2 Report Structure

Chapter 2 reports results of the site investigation carried out prior to the static load tests. The profiles of the CPT cone resistance q_c and SPT blow counts N_{SPT}, along with the basic soil properties obtained from laboratory tests on soil samples collected from the field played an important role in the interpretation of the static load test results.

Chapter 3 presents details of the pile instrumentation for the closed-ended and open-ended test piles. A hybrid instrumentation scheme, involving the installation of both electrical-resistance and the vibrating-wire strain gauges, was used for both test piles. The chapter includes the strain gauge layouts on the test piles, gauge installation and protection procedures and steps followed to assemble the double-wall system for the open-ended test pile.

In Chapter 4 and Chapter 5, pile driving records and static load test results for the closed-ended and open-ended test piles, respectively, are reported. The results include profiles of blow counts, plug measurement for the open-ended test pile, load-settlement curves, resistance components measured at different settlement levels, and profiles of the residual loads and unit shaft resistance.

Chapter 6 compares the behavior of the closed-ended and open-ended piles during pile driving and static load tests. The side-by-side static load tests for the two densely instrumented piles of different types (with almost identical outer diameter and installed in the same soil profile) provide a rare and valuable case history for the foundation community.

Chapter 7 summarizes the main contents and findings presented in the report.

2. SITE INVESTIGATION

2.1 In Situ Tests

The test site was located on the east bank of the Wabash River at its intersection with Sagamore Parkway. Figure 2.1 shows the results of two standard penetration tests (SPTs) and three-cone penetration tests (CPTs) performed near the static pile load testing location. Disturbed soil samples were collected from various depths of the soil profile using a split-spoon sampler during the SPTs. As shown in Figure 2.1, the gravel content (with gravel defined as particles larger than 4.75 mm) is lower than 20% at most depths above z = 16 m (52 ft), except in a thin layer at z = 9 m (30 ft) where high gravel content (above 50%) was found. Then, from z = 16 m (52 ft) to 35 m (115 ft), the gravel content is mostly greater than 30%, and as high as 50%–60% at certain depths. The high gravel content present in the soil profile made it challenging to push the CPT cone (even when using a cone with a diameter of 44.6 mm (1.75 inch)) through these gravelly layers. Therefore, whenever it was not possible to push the CPT cone through a hard soil layer, the cone was retracted to the ground surface, and a string of hollow-stem augers was used to drill through it. The CPT then advanced through the center of the augers until the next hard layer was found. This drill-and-push procedure was repeated as needed until the desired boring depth was reached. Because of the logistical difficulties with such a procedure, it was used only for CPT-3, for which a penetration depth of 33 m (108 ft) was reached; (this depth is greater than the embedment depths of both the test piles). The water table was found at a depth of 3.05 m (10 ft) below the ground surface at the time of the static load test.

2.2 Laboratory Tests

Soil samples, as shown in Figure 2.2, collected from the construction site were tested in laboratory to obtain their basic properties. Figure 2.3 shows the grain size distributions of the soil samples collected at various depths. Table 2.1 provides a summary of the basic soil properties of each soil layer in the soil profile, which consists mainly of poorly graded sand and gravel mixtures.

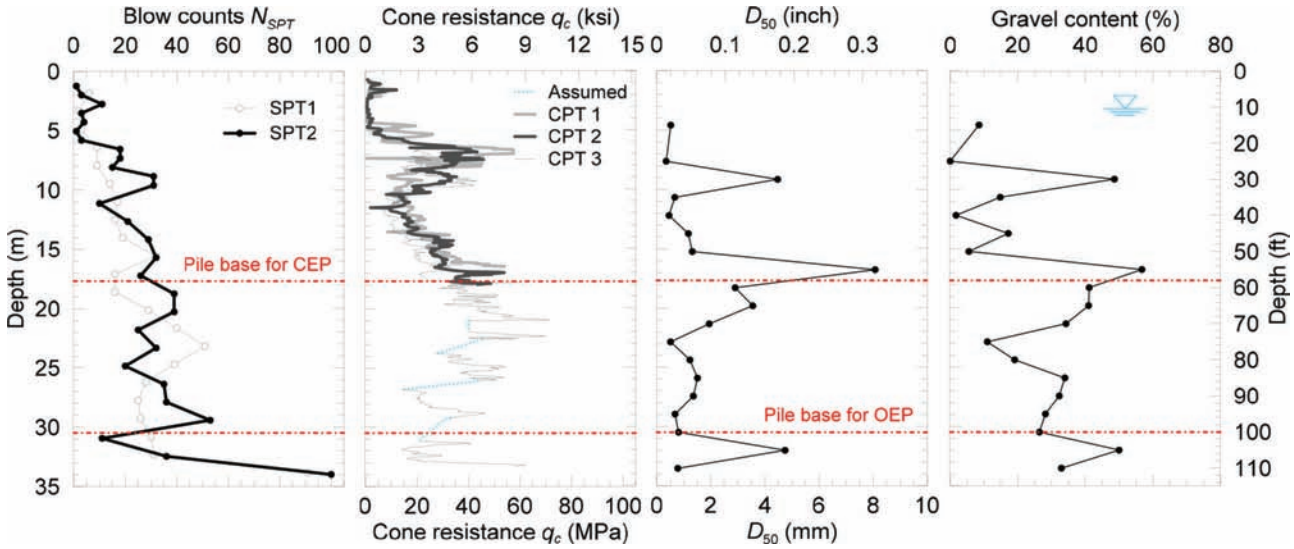

Figure 2.1 In situ test results: blow counts N_{SPT}, cone resistance q_c, mean particle diameter D_{50}, and gravel content (the pile base elevation for the two test piles are shown for reference. (Modified after Han, Ganju, Salgado, & Prezzi, in press b.)

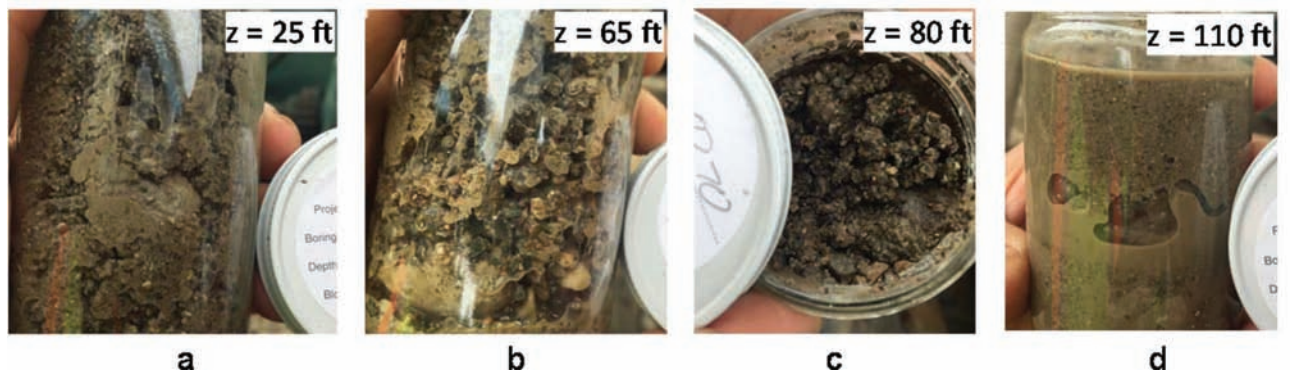

Figure 2.2 Soil samples collected using a split-spoon sampler during the SPTs.

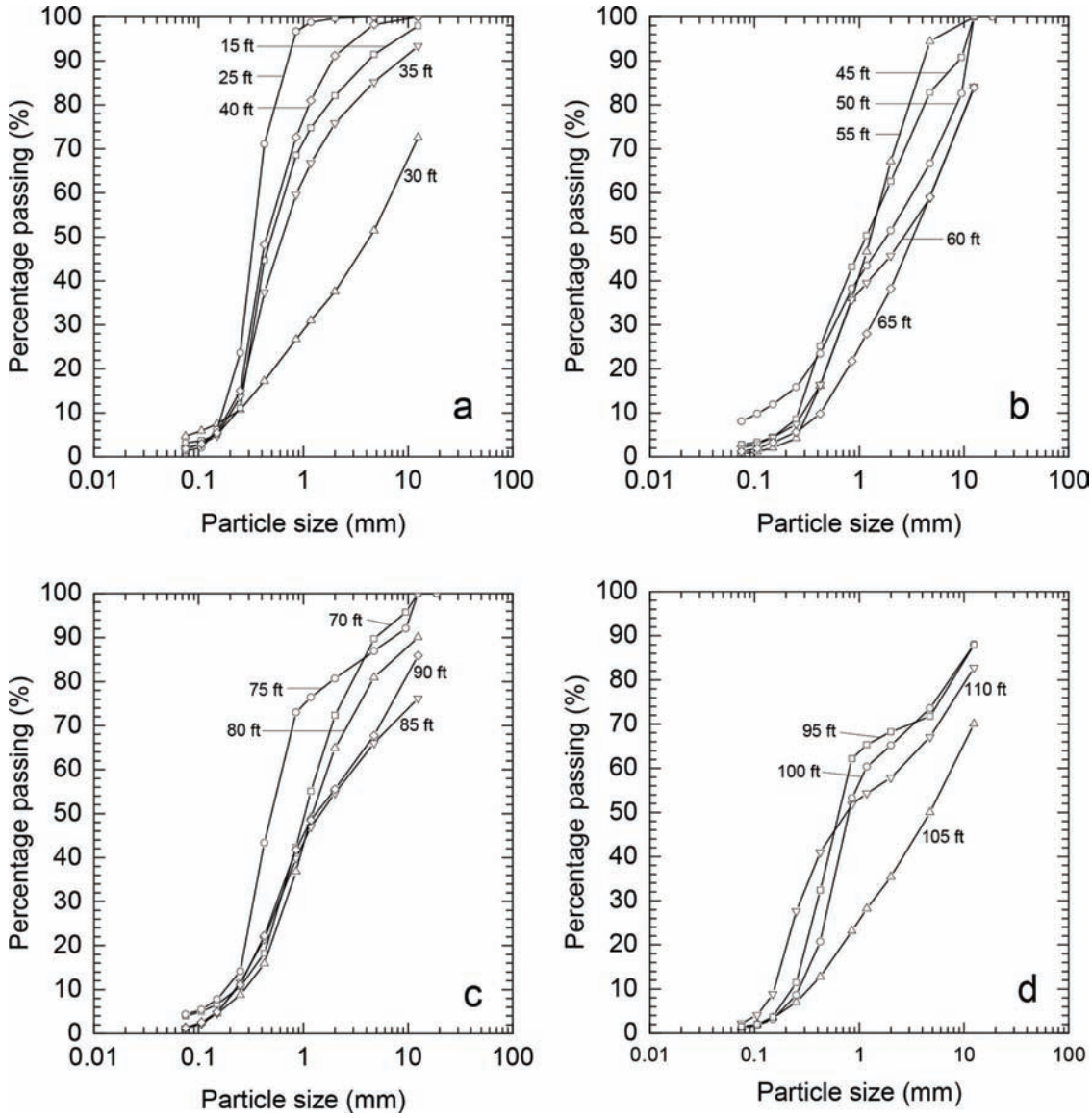

Figure 2.3 Grain size distributions of soil samples obtained from the test site at various depths. (Modified after Han, Ganju, Salgado, & Prezzi, in press b.)

TABLE 2.1
Soil profile at the test site

Layer no.	Depth (ft)	Soil description	γ_t (kN/m^3)	γ_t (lb/ft^3)	Gravel content (%)	D_{50} (mm)	D_{50} (inch)	C_U	C_C	USCS classification
1	0–18	Clayey silt with sand	19.5	125	0	—	—	3.0	0.8	—
2	18–27	Sand with gravel	20.0	128	4	0.4	0.02	2.6	0.9	SP
3	27–34	Sandy gravel	21.5	138	49	4.5	0.18	34.6	0.7	SP
4	34–55	Sand with gravel	20.0	128	10	0.9	0.04	4.8	0.7	SP
5	55–74	Gravely sand	21.5	138	43	4.1	0.16	16.6	0.6	SP
6	74–107	Gravely sand	21.5	138	28	1.1	0.04	8.3	0.8	SP

Source: Modified after Han, Ganju, Salgado, & Prezzi, in press b.

γ_t = total unit weight, D_{50} = mean particle diameter, C_U = coefficient of uniformity = D_{60}/D_{10}, C_C = coefficient of curvature = $(D_{30})^2/(D_{10} \times D_{60})$.

3. INSTRUMENTATION OF THE TEST PILES

3.1 Double-Wall System for the Open-Ended Pile

The axial load Q applied at the head of an open-ended pipe pile is balanced by three resistance components: the outer shaft resistance Q_s, the inner shaft resistance Q_{plug} provided by the soil plug, and the annulus resistance Q_{ann} at the pile base:

$$Q = Q_s + Q_{plug} + Q_{ann} \tag{3.1}$$

In order to properly understand open-ended pipe pile resistance mobilization, these three components of the pile bearing capacity should be independently measured in static load tests. Full instrumentation of closed-ended pipe piles with flat or conical bases involves attaching diametrically opposed strain gauges at regularly spaced intervals along the entire pile length. As the pile is loaded, strains measured at each depth by these gauges are used to calculate the forces acting on the corresponding pile cross-sections and to obtain the load transfer curves for each load increment at the pile head (Abu-Farsakh, Haque, & Tsai, 2017; Bica, Prezzi, Seo, Salgado, & Kim, 2014; Fellenius, Harris, & Anderson, 2004; Han, Prezzi, Salgado, & Zaheer, 2017; Jardine, Zhu, Foray, & Yang, 2013; Kim, Bica, Salgado, Prezzi, & Lee, 2009; Li, Stuedlein, & Marinucci, 2017; Paik, Salgado, Lee, & Kim, 2003; Paik & Salgado, 2003; Seo, Prezzi, & Salgado, 2013; Seo, Yildirim, & Prezzi, 2009). The derivative (slope) of the load transfer curve with respect to depth divided by the pile perimeter gives the magnitude of the unit shaft resistance: a steeper slope indicates greater unit shaft resistance. Such an instrumentation scheme would not work for an open-ended pile since it would not allow independent measurement of the shaft resistances mobilized along the inner and outer surfaces of the pile, for which a double-wall open-ended pipe pile with instrumentation on both the inner and the outer pipes is needed. Two types of double-wall systems have been mentioned in the literature: one with the two concentric pipes connected at the pile base (Finlay, White, Bolton, & Nagayama, 2001), and the other with the two pipes connected at the pile head (Igoe, Gavin, & O'Kelly, 2011; Iskander, 2011; Lehane & Gavin, 2001; Paik et al., 2003; Paik & Lee, 1993; Paik & Salgado, 2003). The second type of instrumentation, as shown Figure 3.1, was used in the present study. The two concentric pipes (one with slightly smaller diameter than the other) were connected at the pile head but not at the base. A pile shoe was connected to only one of the pipes (to the inner pipe in this case). This way, the inner and outer pipes strain independently when an axial load Q is applied at the pile head. This can be better understood by considering the force balance at three cross sections of interest, as shown in Figure 3.1. The axial force at cross section A (at the top of the outer pipe) is balanced by the outer shaft resistance Q_s. The axial force at cross section B (at the top of the inner pipe) is balance by the summation of Q_{ann} and the inner shaft resistance,

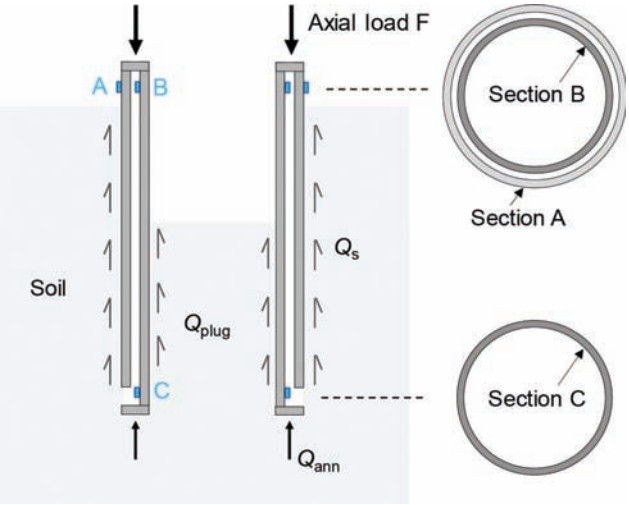

Figure 3.1 Double-wall pipe system to separate measurements of the inner and outer resistance for an open-ended pile. (Modified after Han, Ganju, Prezzi, Salgado, & Zaheer, 2019.)

which is in balance with the compressive stress at the base of the plug, known as the plug resistance Q_{plug}. The axial force at cross section C (near the base of the inner pipe) is balanced by the annulus resistance Q_{ann}. Therefore, strain measurements at these locations provide independent measurement of the three components (Q_s, Q_{ann}, and Q_{plug}) of the axial bearing capacity of an open-ended pipe pile. A detailed profile of the axial load and the throughout the pile length can be obtained by installing a series of strain gauges along the entire pile length.

3.2 Instrumentation Schemes

The instrumentation of the two test piles was carried out in Bowen Laboratory, Purdue University before they were delivered to the test site. A hybrid instrumentation scheme, involving the installation of both electrical-resistance and the vibrating-wire strain gauges, was used for both test piles. Bica et al. (2014) provided a detailed review of the advantages and disadvantages of these two strain gauge types. Figure 3.2 shows the dimensions of the test piles and the locations of the strain gauges installed on them. All strain gauges were installed on the piles in pairs positioned diametrically opposite to each other at specified cross sections of the test piles; this was done so that the strains measured during loading by any strain gauge pair could be averaged to exclude the effect of bending moments on axial strain measurement. The closed-ended test pile was instrumented in a single, 18.3-m-long segment (60 ft), whereas the open-ended test pile was instrumented in two segments (top and bottom segments) of 18.3 m in length (60 ft) due to transportation limitations for pile length. Table 3.1 summarizes the dimensions of the test and reaction piles and the number and type of strain gauges installed on each pile.

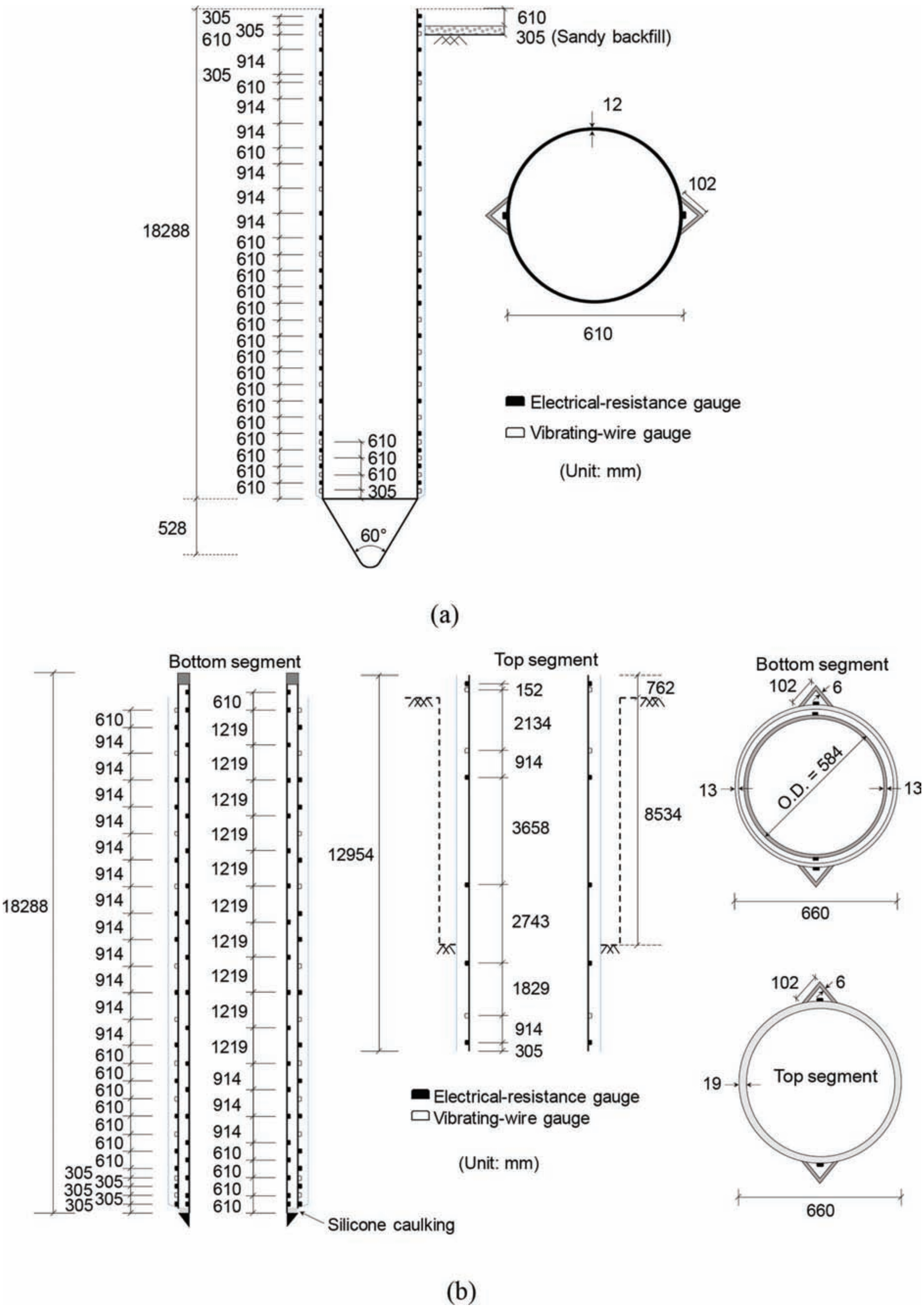

Figure 3.2 Dimensions and the instrumentation details for the (a) closed-ended test pile and (b) open-ended test pile. (Modified after Han, Ganju, Prezzi, Salgado, & Zaheer, 2019; Ganju, Han, Prezzi, & Salgado, 2019.)

TABLE 3.1
Dimensions of the test piles and reaction piles

	Outer diameter (inch)	Inner diameter (inch)	Wall thickness (inch)	Embedment depth (ft)	Number of ER	Number of VW
Closed-ended test pile	24	23	0.5	58	40	24
Open-ended test pile	26	22[1]	2	100	76	28
Open-ended reaction piles	24	23	0.5	125–127	0	0

Source: Modified after Han, Ganju, Salgado, & Prezzi, in press b.
[1]The inner diameter of the bottom segment (double-wall system) of the open-ended test pile.
ER = electrical-resistance strain gauge, VW = vibrating-wire strain gauge.

Figure 3.3 Instrumentation details of the closed-ended test pile. (Modified after Han, Ganju, Salgado, & Prezzi, in press b.)

Figure 3.4 Closed-ended test pile and open-ended test pile (top and bottom segments) with instrumentation completed. (Modified after Han, Ganju, Salgado, & Prezzi, in press b.)

3.3 Instrumentation Procedures

After surface preparation at the desired locations, the closed-ended test pile was instrumented with electrical-resistance strain gauges (Tokyo Sokki Kenkyujo Model FLA-6-350-11-3LT) and vibrating-wire strain gauges (Geokon Model 4000) following recommended gauge installation procedures (Han, Prezzi, Salgado, & Zaheer, 2017). All the steps required for proper installation of the electrical-resistance strain gauges were described by Han et al. (Han, Prezzi, Salgado, & Zaheer, 2017; Han, Ganju, Prezzi, Salgado, & Zaheer, 2019). Mineral wool was carefully wrapped around the gauge cables collected along the length of the pile so that the welding of steel angles onto the pile (see Figure 3.3) could proceed without risk of excessive heat damaging the gauges and cables. The channels protected the gauges and cables from damage during transportation and driving operations. A steel conical driving shoe (with an apex angle of 60 degrees) was welded to the base of the pile to improve drivability in the gravelly sand layers of the soil profile (see Figure 3.4).

The open-ended test pile was composed of two pipe segments welded in the field. The estimated length of the soil plug that would form during driving was smaller than the length of the bottom segment (=18.3 m = 60 ft). Therefore, a double-wall system was used only for the bottom segment of the pile. Since the gap between the inner and outer pipes forming the double-wall system of the bottom segment was only 25 mm (1 inch) (see Figure 3.2b), only electrical-resistance strain gauges were placed on the inner pipe (vibrating-wire gauges would no fit there). To allow proper assembly of the inner and outer pipes of the double-wall system, steel spacing rods of 10 mm (0.4 inch) in diameter were welded on the outer surface of the inner pipe along its length (see Figure 3.5a); the diameter of the steel spacing rods was greater than the diameter of the gauge cables (= 4.3 mm = 0.17 inch). The electrical resistance strain gauges were installed, and their cables were tightly arranged and fixed in between the spacing rods using super glue and Gorilla® tape. A hardened steel cutting shoe (Versa-Steel Inc. VS700 series 196) was welded to the base of the inner pipe. A pair of high-capacity nylon wheels mounted at the top end of the inner pipe (see Figure 3.6a) and an overhead crane (see Figure 3.6b) were used to facilitate the sliding of the inner pipe into the outer pipe to build the double-wall pile. The instrumentation of the outer pipe of the bottom pile segment and the single pipe of the top pile segment was similar to that of the closed-ended test pile, with both electrical-resistance and vibrating-wire strain gauges installed.

After sliding, the inner and outer concentric pipes were connected at the top by welding them to two

steel rings (one with thickness = 13 mm, I.D. = 584 mm (23 inch) and O.D. = 634 mm (25 inch), and the other with thickness of 51 mm = 2 inch, I.D. = 558 mm = 22 inch and O.D. = 660 mm = 26 inch). The 76 mm (3 inch) gap between the outer pipe and the cutting shoe (welded on the inner pipe) was filled with silicone (Figure 3.6c), which is deformable when compared with steel. Thus, the two pipes could strain independently upon loading. As shown in Figure 3.6c, four centering bolts with a diameter of 25.4 mm (1 inch) were screwed in through the outer pipe and pushed on the inner pipe to make the pipes concentric during storage and transportation. When the pile was stored in the horizontal position, the weight of the inner pipe was supported by the connection with the outer pipe on the top end and the centering bolts on the bottom end of the double-wall system. The centering bolts were removed immediately before pile driving. Figure 3.4 shows all the pile segments with completed instrumentation before they were delivered to the test site.

3.4 Measurement for the Plug Formation

The response of open-ended pipe piles to axial loading depends on plug formation during driving. As an open-ended pipe pile is driven into the ground, soil enters the pile through the opening at the bottom; the soil inside the pile plays an important role in resistance mobilization both during driving and in static loading (Igoe et al., 2011; Lehane, Schneider, & Xu, 2005b; Paik & Salgado, 2003). The load response of an open-ended pipe pile is closely related to the formation of the soil plug during pile driving. Researchers have proposed equations to estimate the axial bearing capacity of open-ended pipe piles as a function of plug parameters (e.g., the incremental filling ratio IFR and the plug length ratio (PLR)) (Lee, Salgado, & Paik, 2003; Lehane et al., 2005b; Paik & Salgado, 2003).

Figure 3.7 shows a weight system that was used to measure the development of a soil plug during driving of an open-ended pipe pile. Two different weights were connected to the two ends of a string that passes through a horizontal pipe welded about 1*B* below the pile head. The larger weight is placed on top of the soil plug inside the pipe pile, and the smaller weight is left

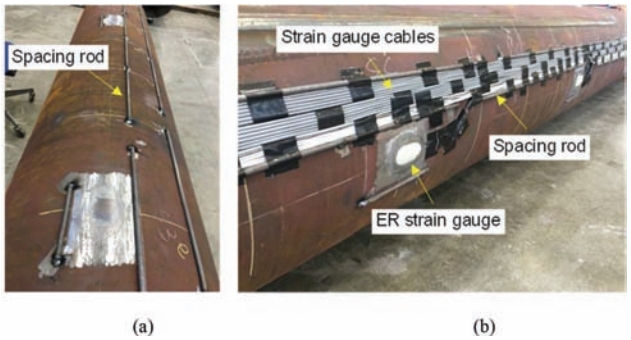

Figure 3.5 Instrumentation details for the inner pipe of the bottom segment for the open-ended test pile: (a) spacing rods welded on the surface of the inner pipe; (b) arrangement of the strain gauges and their cables on the inner pipe. (Modified after Han, Ganju, Salgado, & Prezzi, in press b.)

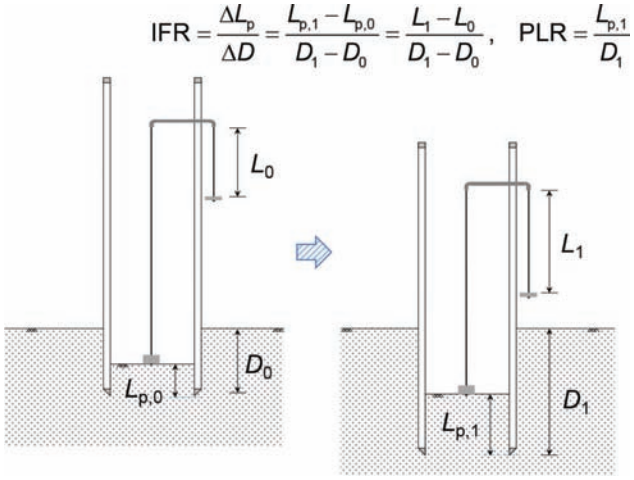

Figure 3.7 Measurement scheme for the plug formation. (Modified after Han, Ganju, Prezzi, Salgado, & Zaheer, 2019.)

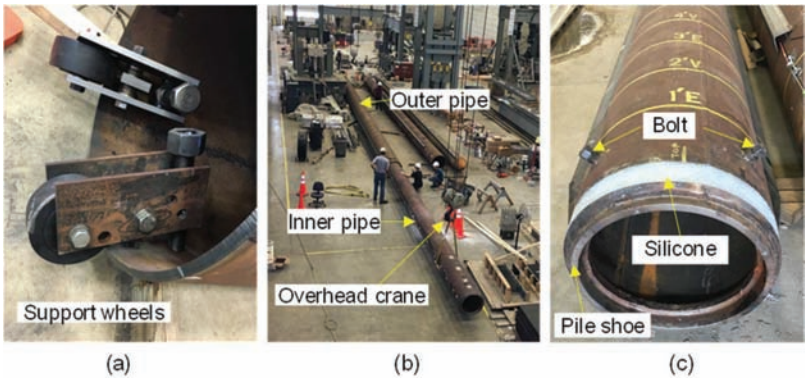

Figure 3.6 Assembly of the double-wall system for the open-ended test pile: (a) two support wheels attached to the top of the inner pipe; (b) sliding of the inner pipe into the outer pipe with the assistance of the overhead crane; (c) base of the open-ended test pile. (Modified after Han, Ganju, Salgado, & Prezzi, in press b.)

hanging outside the pile. When the pile is driven from an initial state at a depth L_0 to a new state L_1, the plug length L_p increases from $L_{p,0}$ to $L_{p,1}$ for an increment ΔL_p of pile penetration, and the length of the string hanging outside of the pile will accordingly increase by the same amount. Thus, the plug length increment ΔL_p can be easily measured as the change of position of the smaller weight (hanging outside the pile) with respect to tick marks of a scale painted on the pile outer surface.

4. STATIC AND DYNAMIC LOAD TESTS OF THE CLOSED-ENDED PIPE PILE

4.1 Pile Installation

The CEP was initially driven into the ground to a depth of 17.37 m (57 feet) using a single-impact diesel hammer (Model No. APE D70-52) on October 4, 2016 (see Figure 4.1). The hammer has a ram weight of 68.7 kN (15.4 kip), maximum capacity of 235 kN-m (173,327 ft-lbs.) and a maximum stroke length of 3.4 m (11.15 ft). Strain readings from ER gauges were recorded at the end of driving to obtain the locked-in residual loads due to pile driving. After driving, 0.3 m (1 ft) of sandy backfill was added to elevate the ground surface to accommodate the loading frame and the supporting machinery. As a result, the final embedment depth of the pile became 17.68 m (58 ft).

Figure 4.2 shows the driving resistance profile (blow counts per meter of pile penetration as a function of depth) recorded during driving. For the top 5 m (16.4 ft), the driving resistance through the clayey silt layer was low (less than 4 blows/m). The driving resistance increased for penetration depths greater than 6 m (19.7 ft) as the CEP started to sense the dense gravelly-sand layers. A peak in driving resistance (110 blows/m = 33 blows/ft) was observed at a penetration depth of 7.5 m (24.6 ft), which was followed by a small drop and then a monotonic rise thereafter to about 100 blows/m (30 blows/ft) at the final penetration depth of 17.37 m (57 ft) from the ground surface.

4.2 Static Load Test

Figure 4.3 shows a schematic of the front and top views of the load frame and settlement measurement setups for the SLT. Load was applied on the head of CEP using a 2-MN-capacity hydraulic jack (Model No. ATF-Model-24). The reaction for the hydraulic jack was obtained from a loading frame attached to eight open-ended piles with outer diameter of 610 mm (24 in). To ensure capacity, each open-ended reaction pile was driven to a minimum depth of 36.6 m (120 ft). The positions of the reaction piles were chosen to have a minimum distance of 5*B* between the CEP and the reaction piles, in accordance with ASTM (2013).

Figure 4.1 CEP being driven into the ground with a single-impact diesel hammer positioned on the top and a guiding frame around the CEP to ensure verticality during driving. (Modified after Ganju et al., 2018.)

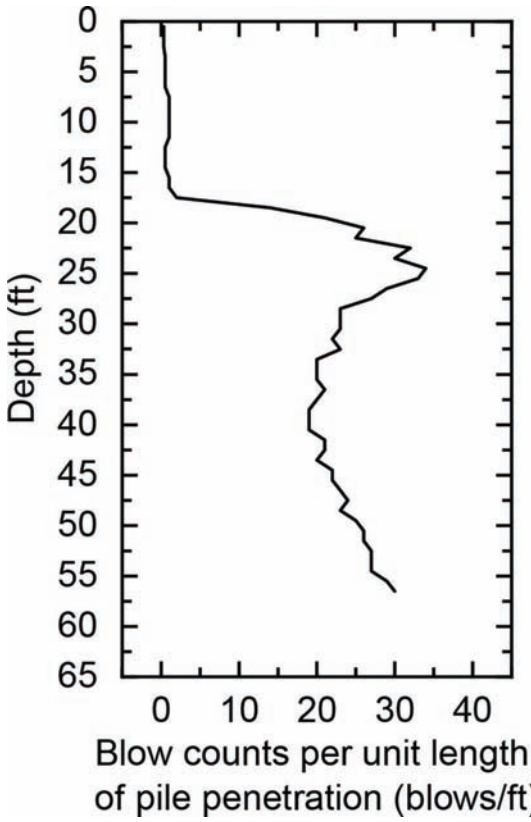

Figure 4.2 Driving resistance for CEP verses depth. (Modified after Ganju et al., 2018.)

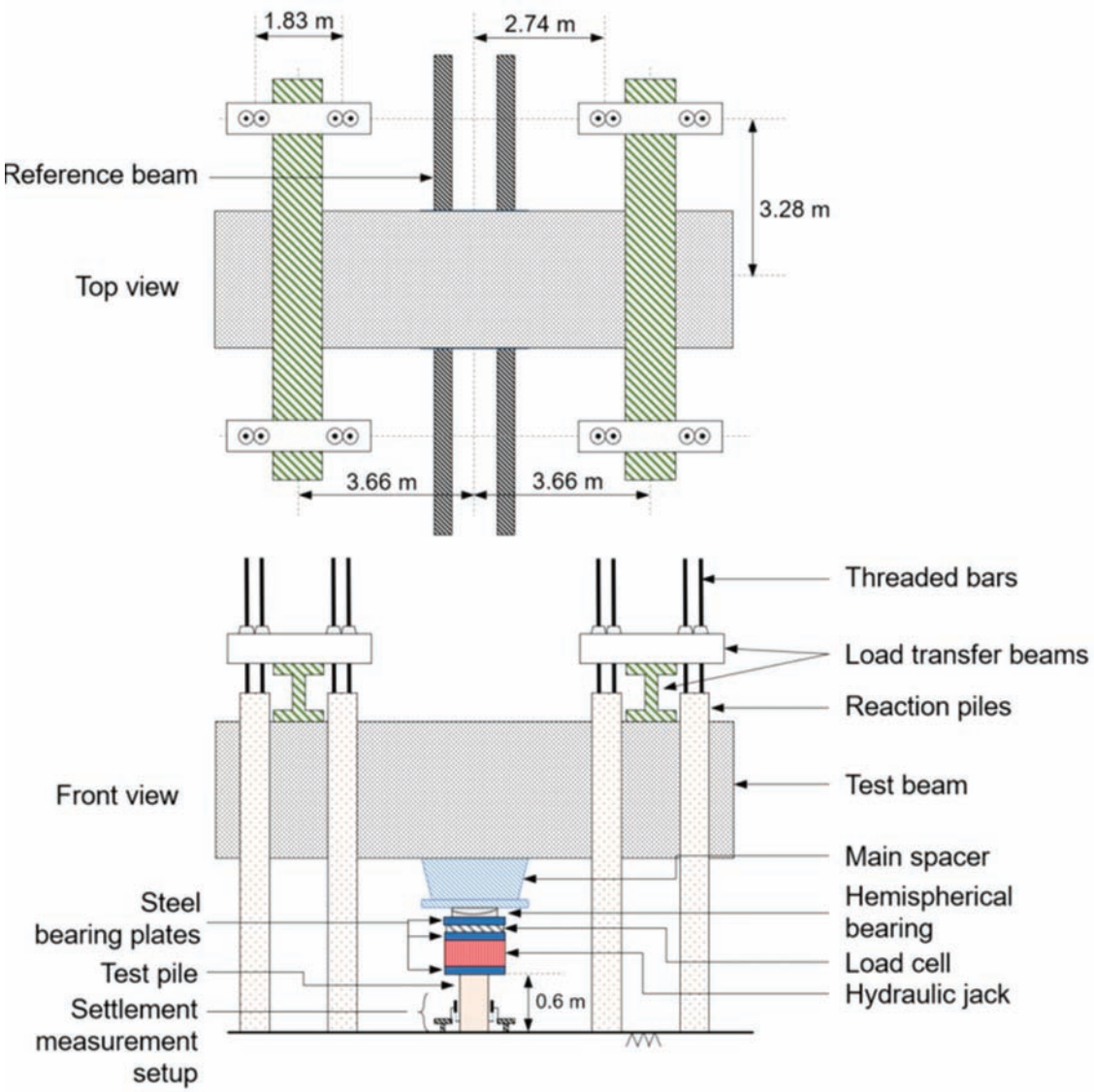

Figure 4.3 Top and front view of the SLT loading frame and settlement measurement system. (Modified after Ganju et al., 2018.)

A recently calibrated load cell was used to measure the loads applied by the hydraulic jack to the CEP head during the SLT. To prevent any application of eccentric loading at the pile head, all the components of the loading frame were properly aligned, and a hemispherical bearing was placed between the reaction frame and the load cell. Four digital dial gauges mounted on reference beams were used to measure the vertical settlements at the pile head. The reference beams were anchored sufficiently far from the CEP and the reaction piles so as not to be affected by ground movement. Measurements from the four dial gauges agreed throughout the SLT, indicating minimal inclined settlement.

The SLT was carried out on October 17, 2016, 13 days after the CEP was driven and lasted 36 hours. Prior to start of the SLT, the ER and VW gauges were zeroed. The SLT was carried out as a slow-maintained test with small load increments to get a complete definition of the load-settlement curve all the way to the plunging load. A strict loading criterion was followed during the SLT: a load increment was applied at the pile head, and the resulting settlement was measured at zero, one, two, five, and ten minutes and every ten minutes thereafter for a period of up to two hours. The next load increment was applied when the rate of settlement was smaller than 0.25 mm/hour (the settlement rate was calculated from two consecutive settlement readings). Whenever the settlement rate was not below the 0.25 mm/hour threshold within the prescribed 2-hour period, the next load increment was halved and applied when the settlement difference between two consecutive settlement readings was less than 5%. These applied load increments [maximum of 444.8 kN (100 kips)] were considerably smaller than the four equal increments proposed by ASTM (2013).

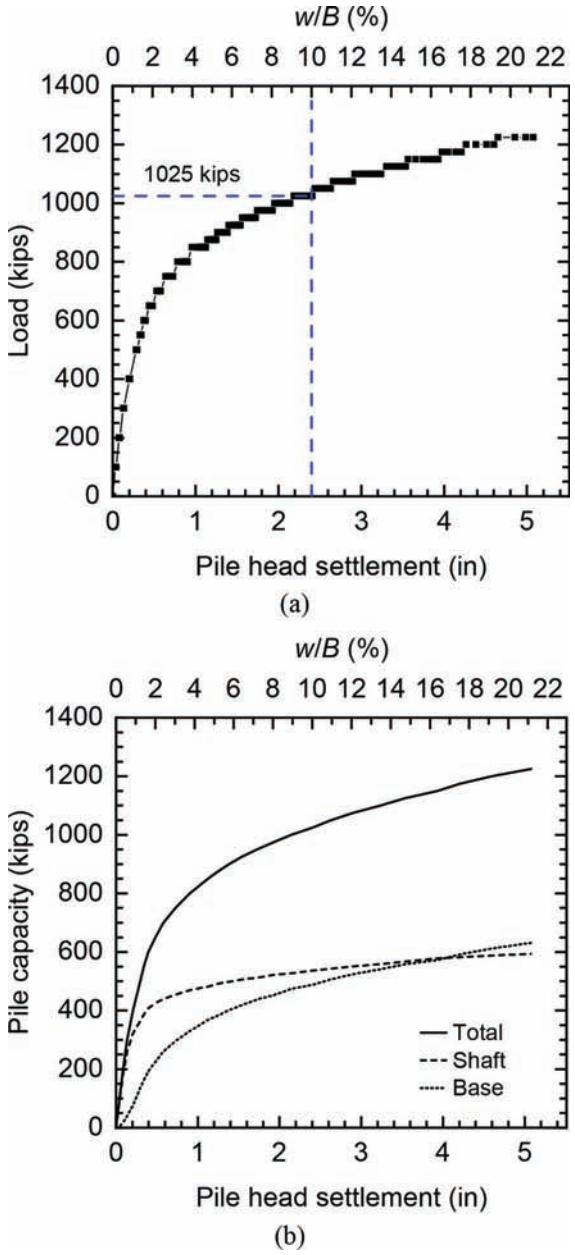

Figure 4.4 Static load test results: (a) load-settlement curve; (b) total, base and shaft capacity components plotted against pile head settlement w and relative settlement w/B. (Modified after Ganju et al., 2018.)

Figure 4.4a shows the load-settlement curve obtained from the SLT. At each load level, several settlement readings were taken, as described above. A load increment of 444.8 kN (100 kips) was used until a load of 2,224.1 kN (500 kips) was reached. The load increments were then decreased to 222.4 kN (50 kips) until the load level of 3,781.0 kN (850 kips). The load increments were further decreased to 111.2 kN (25 kips) thereafter, all the way to the plunging load of 5449 kN (1225 kips). This allowed us to better define the ultimate capacity of the pile at $0.1B$ settlement and prevent excessive rate of settlement as the pile approached its plunging load. Plunging was assessed to occur when the settlement rate was greater than 50 mm/hour. After the plunging load, the pile was unloaded in four equal decrements with a waiting period of 15 min between each load decrement.

With the strain gauge measurements along the pile shaft and the total applied load, the shaft and base capacity of the pile were calculated. These are shown in Figure 4.4b as a function of pile head settlement w and relative settlement w/B. The load-settlement response of the CEP was almost linear up to a load of 2,891 kN (650 kips), corresponding to $w/B = 0.02$ (w=12.2 mm); at this settlement level, 65% of the total capacity of the CEP came from the shaft (1,891 kN = 425 kips) and 35% from the base (1,000 kN = 225 kips). Upon further loading, the shaft capacity stabilized, with the additional load increments taken mostly by the base of the CEP. At $w/B = 0.05$ (w = 31.7 mm), 56% (2,189 kN = 492 kips) of the total capacity of the CEP pile (3,892 kN = 875 kips) was transferred to the surrounding soil by the shaft and 44% (1,703 kN = 383 kips) by the base.

The ultimate capacity, defined as the total capacity at the pile head when $w/B = 0.1$ (Clausen, Aas, & Karlsrud, 2005; Han, Prezzi, Salgado, & Zaheer, 2017; Jardine, Chow, Overy, Standing, & Jamie, 2005; Kolk, Baaijens, & Senders, 2005; Lehane et al., 2005b; Salgado, 2008), was equal to 4,559 kN (1,024 kips), which was approximately equally distributed between the shaft (2,389 kN = 537 kips) and base (2,171 kN = 488 kips). With additional load increments, the base capacity surpassed the shaft capacity at a total load level of about 5,227 kN (at $w/B = 0.175$; w = 106.9 mm). Shortly thereafter, the pile started to plunge at a total load of 5,449 kN (1,225 kips) (corresponding to $w/B = 0.212$).

4.3 Residual Loads

Immediately after pile driving, the pile tends to recover the compressive strain induced by driving, and the soil below the pile base tends to rebound. The soil surrounding the pile shaft resists the relative movement between the pile and the soil through interface friction, resulting in locked-in residual axial loads in the pile (Alawneh & Malkawi, 2000; Briaud & Tucker, 1984; Fellenius, 2002; Han, Prezzi, Salgado, & Zaheer, 2017; Kim et al., 2009; Paik et al., 2003). The residual loads do not affect the total measured capacity of the pile; however, they do affect the distribution of the total capacity into shaft and base components.

The residual loads in the CEP after pile driving were measured by zeroing all the ER gauges prior to driving and taking strain measurements immediately after driving. The VW gauges were not used for residual load measurements, as these tend to drift during driving due to micro-slippages between the sensor coil and the sensor bar due to inertial forces (Bica et al., 2014). The residual loads and the unit shaft friction measured at the end of driving are shown in Figure 4.5a and b,

respectively. The residual loads in the pile were compressive throughout the length of the pile. At the head of the pile, which was above the ground surface, the residual axial loads were zero. A maximum residual load of 420 kN (94.4 kips) was measured at a depth of 12 m (39.4 ft) from the ground surface, while, at the pile base, a load of 233 kN (52.4 kips) was recorded. The resulting unit shaft friction above 12m (39.4 ft) depth was negative (pointing downwards), and from 12 m (39.4 ft) to the pile base at 17.68 m (58 ft), it was positive (pointing upwards). For about 70% of the pile length, the unit shaft friction arising from the residual loads was negative.

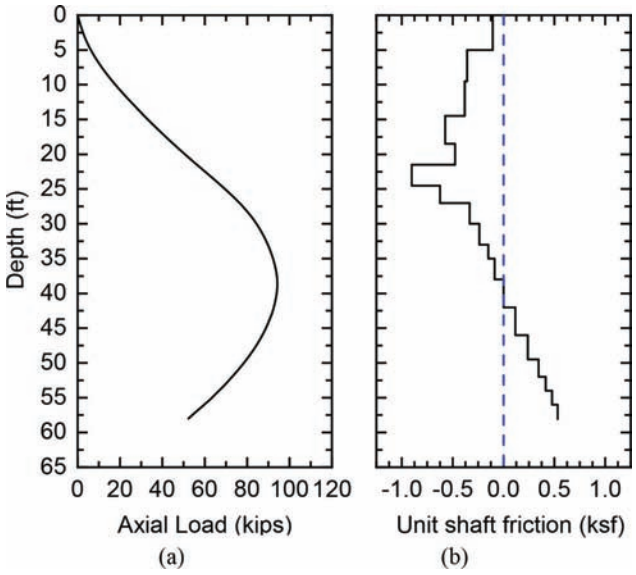

Figure 4.5 Residual loads at the end of pile driving: (a) profile of the residual loads in pile at different depths; (b) profile of the residual unit shaft friction. (Modified after Ganju et al., 2018.)

4.4 Shaft and Base Capacities

Since the strain gauges were re-zeroed prior to the SLT, the loads measured during the SLT do not account for the locked-in residual loads developed during pile driving. The true loads in the pile are the summation of the axial loads measured during the SLT and the locked-in residual loads measured at the end of driving. Figure 4.6a shows for the loads corresponding to $w/B = 0.1$ (ultimate limit state): the residual loads measured at the end of driving, the axial loads measured during the SLT and the axial loads corrected for the residual loads. Figure 4.6b shows the corresponding unit shaft friction profiles with and without correction for residual loads.

The unit shaft friction corrected for residual loads are mostly lower than the uncorrected unit shaft friction because for about 70% of the pile shaft (from 0 m to 12 m depth, or from 0 ft to 39 ft), the residual unit shaft friction is negative. For 30% of the pile shaft (from 12 m to 17.68 m depth, or from 39 ft to 58 ft), the residual unit shaft friction is positive and therefore results in slightly higher corrected unit shaft capacity. Correction for the residual loads resulted in about 10% drop in the limit shaft capacity from 2,389 kN (537 kips) to 2,156 kN (485 kips), and about 10% increase in the ultimate base capacity from 2,170 kN (488 kips) to 2,403 kN (540 kips).

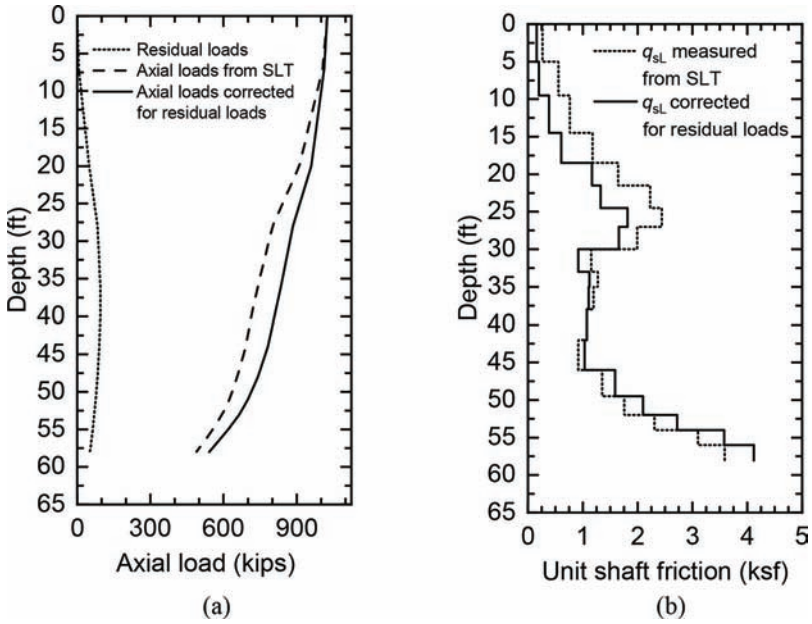

Figure 4.6 Consideration of residual loads for loads measured at $w/B = 10\%$: (a) axial load transfer curves; (b) unit shaft friction profiles. (Modified after Ganju et al., 2018.)

4.5 Comparison of Measured and Predicted Pile Capacity

The ultimate unit base capacity $q_{b,ult}$ of a pile is often calculated as a fraction of the CPT tip resistance q_c averaged near the depth of the pile base. The relationship between $q_{b,ult}$ and q_c is presented in design equations as a function of the relative density of the soil (Han, Prezzi, Salgado, & Zaheer, 2017; Salgado, Woo, & Kim, 2011), diameter of the pile (Jardine et al., 2005) or the vertical effective stress at the depth of the pile base (Clausen et al., 2005). The ratio of the measured unit base capacity q_b to average cone resistance near the pile base $q_{cb,avg}$, at different settlement levels during the SLT, is shown in Table 4.1. This ratio ranges from 0.23 to about 0.36, with a value of 0.29 at the ultimate limit state. The literature however suggests that the value of $q_{b,ult}/q_c$ is generally in the range of 0.3 to 0.8 (Chow, 1997; Lee & Salgado, 1999; Lehane et al., 2005b; Salgado, 2008).

The unit shaft resistance q_{sL} at the pile sand interface is computed as the product of the normal stress σ'_h at the interface and the soil-pile interface friction coefficient tan δ, where δ is the interface friction angle between the soil and pile surface. (Han, Ganju, Salgado, & Prezzi, 2018; Jardine et al., 2005, Jardine, Lehane, & Everton, 1993; Randolph, 2003; Salgado et al., 2011). The normal stress σ'_h at the interface is obtained as the product of the vertical effective stress σ'_v and the coefficient of lateral earth pressure K. K for driven piles, under the given soil conditions is expected to be in the range of 0.5 to 2.5 according to the literature (Fleming, Weltman, Randolph, & Elson, 2008; De Nicola & Randolph, 1993; Salgado, 2008), which matches quite well with the measured values of K shown in Figure 4.7. The q_{sL} is also often calculated as a fraction of the initial vertical effective stress σ'_v ($q_{sL} = \beta\sigma'_v$) or the cone resistance q_c ($q_{sL} = c_s q_c$). The value of β (a proxy for the product of K tan δ) is generally expected to be in the range of 0.25 to 1.8 for drill shafts, a similar value may be expected for driven piles (given that K would be higher and tanδ lower). The ratio of q_{sL} to q_c is expected to be in the range of 0.1 to 1.1 for sands (Randolph, 2003; Salgado et al., 2011), with higher values expected for fine-grained soils, as also observed in Figure 4.7.

With high quality q_c data, more sophisticated design methods can be used to estimate the pile capacity. These methods consider the effect of pile installation, state of the soil *in situ* and the possible effects of pile setup (Bowman & Soga, 2005; Lee, Kim, Salgado, & Zaheer, 2010). As the pile is driven into the ground, the unit shaft friction at a certain depth along the pile decreases as the pile is driven down further. This is due to a reduction in the normal stress on the pile with the increasing number of hammer blows on the pile head. This phenomenon is called friction degradation (White & Bolton, 2002) and is accounted for in some pile design methods by means of a shaft degradation term (Han, Prezzi, Salgado, & Zaheer, 2017; Jardine et al., 2005; Kolk et al., 2005; Lehane et al., 2005b; Randolph, 2003).

As the test pile was driven in a soil profile with large gravel content, sharp peaks in the q_c profile were observed, as seen in Figure 4.8. To mitigate the effect of particle size, a 44.5-mm-diameter (1.75 inch) CPT cone was used during testing. However, at depths where gravel content was observed to be on the higher side (50%), i.e., at depths of 9 m (29.5 ft) and 15–18 m (49–59 ft), sharp peaks and valleys were still observed in the q_c profile. For estimation of pile capacity from the CPT-based pile design methods, these peaks were excluded since these peaks are likely caused due to the cone breaking and/or dragging down gravel particles. A modified "lower bound" CPT, shown in Figure 4.8 alongside the gravel content, was used as the input in the design methods.

The soil properties obtained from the laboratory testing of *in situ* soil samples collected using the split-spoon sampler are presented in Table 4.3. The interface friction angles needed as input in some of the pile design methods were chosen according to the recommendations of Han et al. (2018) and Han, Ganju, Salgado, & Prezzi (in press a). Using the soil properties in Table 4.3, the pile capacities were computed using five of the most commonly used pile design methods available in the literature: (1) Purdue pile design method (Han, Prezzi, Salgado, & Zaheer, 2017;

TABLE 4.1
Comparison of unit base capacity q_b and normalized unit base capacity $q_b/q_{cb,avg}$ at different pile head settlements

Relative pile head settlement	Unit base capacity (MPa)	Unit base capacity (psi)	$q_b/q_{cb,avg}$[1]
0.05B	6.5	943	0.23
0.10B[2]	8.2	1,189	0.29
0.15B	9.3	1,349	0.33
0.21B[3]	10.4	1,508	0.36

Source: Modified after Ganju et al., 2018.
[1]$q_{cb,avg}$ computed as the average q_c 1B above and 2B below the pile base (= 28.7 MPa = 4163 psi).
[2]Ultimate load level.
[3]Plunging load level.

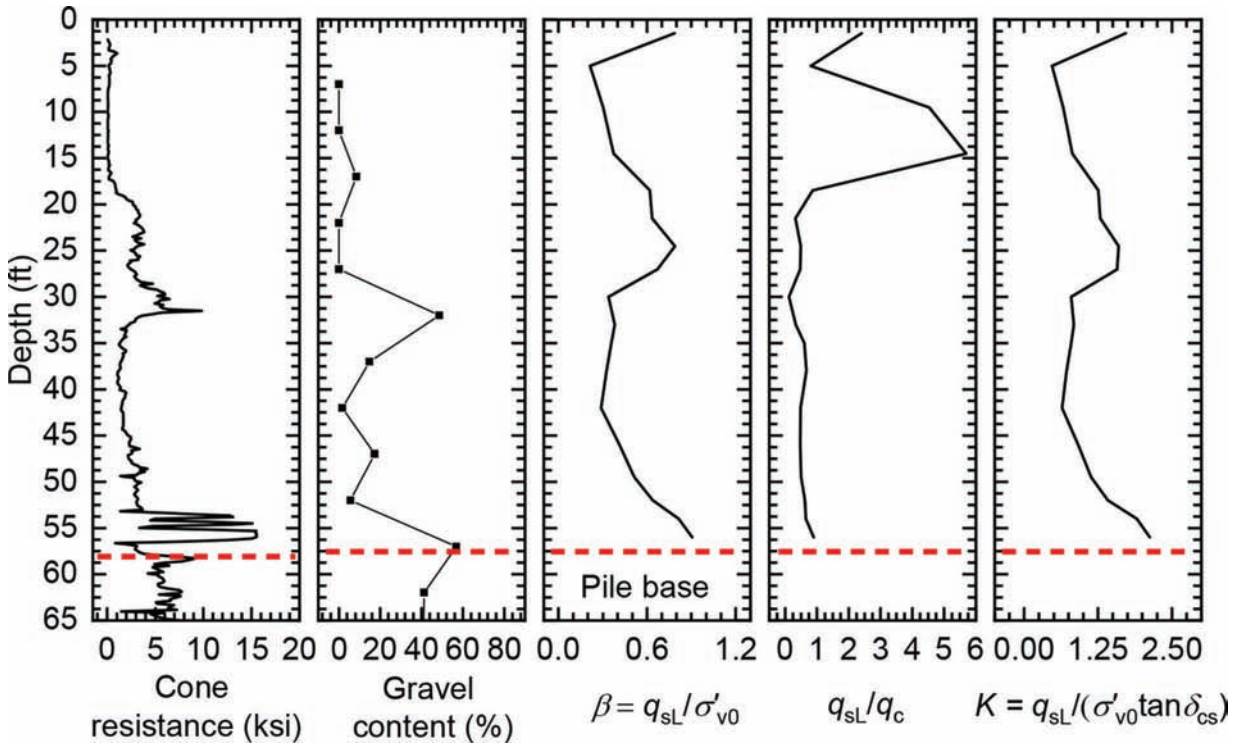

Figure 4.7 Profiles of cone capacity, gravel content, $\beta(=qsL/\sigma'_{v0})$, coefficient of lateral earth pressure $K(=q_{sL}/(\sigma'_{v0}\tan\delta_{cs}))$ and normalized unit limit shaft friction q_{sL}/q_c after correction for the residual loads. (Modified after Ganju et al., 2018.)

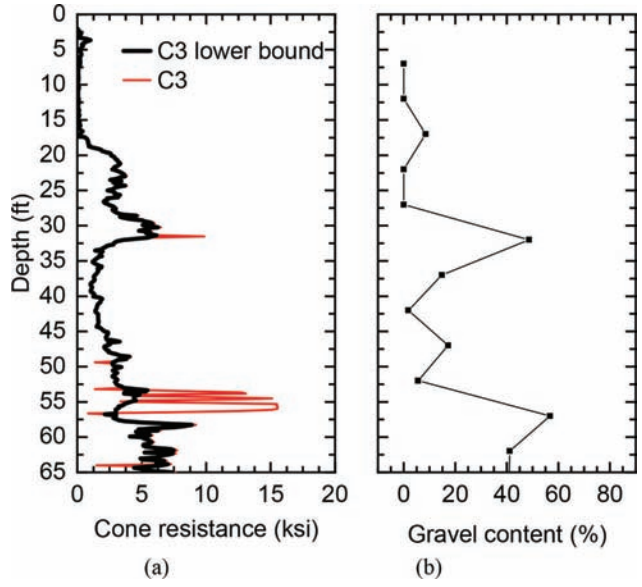

Figure 4.8 High gravel content causes peaks in cone resistance q_c: (a) plot of cone resistance with "lower bound" of cone resistance excluding the peaks; (b) plot of gravel content vs. depth. (Modified after Ganju et al., 2018.)

Randolph, 2003; Salgado et al., 2011), (2) ICP method (Jardine et al., 2005), (3) UWA method (Lehane et al., 2005b), (4) NGI method (Clausen et al., 2005) and (5) Fugro method (Kolk et al., 2005). Table 4.2 summarizes the design equations for these five methods. The capacities computed from the methods are presented in Table 4.4 together with the results from the SLT and pile driving analysis (PDA) results. The PDA results were obtained from GRL engineers.

The unit shaft friction profile computed from each design method and the measured unit shaft friction profile are presented in Figure 4.9. The pile design methods predict the unit shaft capacity accurately, while the unit base capacity is always overpredicted by a factor of about two. Lehane, Schneider, and Xu (2005a) reported similar observations about CPT based pile design methods overestimating the total pile capacity for piles driven in gravelly sands (Briaud, Moore, & Mitchell, 1989; Nevels & Snethen, 1994). As shown in Table 4.5, from the design methods, the $q_{b,ult}$ to $q_{cb,avg}$ ratio is in the range of 0.40–0.60, while the measured ratio is equal to 0.23. The ICP design method produces the smallest ratio, but still it is almost twice the measured value.

The unit base resistance of the pile at the limit state q_{bL} is comparable to the cone resistance q_c measured near the pile base (Salgado, 2008). However, from the SLT data, we observe that the q_{bL} is only one third of the q_c measured at that depth (see Table 4.1). While the measured q_{bL} ($\approx$10 MPa = 1450 psi) may still be in the process of reaching its full value, the measurement of low q_{bL}/q_c ratio (0.36) suggests an overestimation of the q_c under the present soil conditions. The overestimation of $q_{b,ult}$ from design methods may therefore be

TABLE 4.2
Design methods for driven piles in sand

Method and key reference	Limit unit shaft resistance q_{sL}	Ultimate unit base resistance $q_{b,ult}$	Comments
Purdue-CPT (Han, Prezzi, Salgado, & Zaheer, 2017; Han, Ganju, Salgado, & Prezzi, in press b; Randolph, 2003; Salgado et al., 2011)	$q_{sL} = K\sigma'_{v0} \tan \delta_c$ $K = K_{min} + (K_{max} - K_{min}) \exp(-\alpha \frac{h}{B})$ $K_{min} = 0.2$ $K_{max} = 0.01(q_c/P_A)/\sqrt{\sigma'_{h0}/P_A}$ h is the distance from the depth being considered to the pile base; K_{min} = 0.2; α = 0.05.	$q_{b,ult} = (1-0.0058D_R)q_{cb,avg}$	—
ICP (Jardine et al., 2005)	$q_{sL} = (\sigma'_{rc} + \Delta\sigma'_{rd}) \tan \delta_c$ $\sigma'_{rc} = 0.029 q_c \left(\frac{\sigma'_{v0}}{p_A}\right)^{0.13} \left(\frac{h}{R}\right)^{-0.38}$ $\Delta\sigma'_{rd} = 2G\Delta r/R$ $G = q_c\left[0.0203 + 0.00125\eta - 1.216\times10^{-6}\eta^2\right]^{-1}$ $\eta = q_c\left(p_A\sigma'_{v0}\right)^{-0.5}$ Δr = .02 mm for lightly rusted steel piles; h is the distance from the depth being considered to the pile base, $h/R \geq 8$.	$q_{b,ult} = \max[0.3, 1-0.5 \log(B/B_{CPT})]\, q_{cb,avg}$ B_{CPT} is cone diameter = 0.036 m.	Intended to predict the pile bearing capacity 10 days after driving for "virgin" piles.
UWA (Lehane et al., 2005b)	$q_{sL} = \frac{f}{f_c}\left(\sigma'_{rc} + \frac{4G\Delta r}{B}\right) \tan \delta_c$ $\sigma'_{rc} = 0.03 q_c \left[\max\left(\frac{h}{B}, 2\right)\right]^{-0.5}$ $G/q_c = 185\left[\frac{q_c/p_A}{\sigma'_{v0}/p_A}\right]^{-0.75}$ $\Delta r = 0.02\, mm$ f/f_c = 1 for compression and 0.75 for tension.	$q_{b,ult} = 0.6 q_{cb,avg}$	The method is intended to predict the pile bearing capacity measured 10–20 days after driving.
NGI (Clausen et al., 2005)	$q_{sL} = \max\left[p_A\left(\frac{Z}{Z_{base}}\right)\left(\frac{\sigma'_{v0}}{p_A}\right)^{0.25} F_{D_R}F_{tip}F_{load}F_{mat}, 0.1\sigma'_{v0}\right]$ $F_{D_R} = 2.1\left[D^*_R - 0.1\right]^{1.7}$ $D^*_R = 0.4 \ln\left\{\frac{q_c}{22(\sigma'_{v0}p_A)^{0.5}}\right\}$ where z is the depth below the ground surface; z_{base} is the pile base depth; F_{tip} = 1.6; F_{load} = 1.3 for compression; F_{mat} = 1.0 for steel and 1.2 for concrete pile; D^*_R is the nominal relative density, which may be greater than 100%.	$q_{b,ult} = \frac{0.8 q_{cb,avg}}{1 + \left\{0.4 \ln\left[\frac{q_{cb,avg}}{22(\sigma'_{vb}p_A)^{0.5}}\right]\right\}^2}$ σ'_{vb} is the vertical effective stress at the depth of the pile base.	—
Fugro (Kolk et al., 2005)	$q_{sL} = 0.08 q_c \left(\frac{\sigma'_{v0}}{p_A}\right)^{0.05} \left(\frac{h}{R}\right)^{-0.9}$ *if* $h/R \geq 4$ $q_{sL} = 0.08 q_c \left(\frac{\sigma'_{v0}}{p_A}\right)^{0.05} (4)^{-0.9} \left(\frac{h}{4R}\right)$ *if* $h/R < 4$ h is the distance from the depth being considered to the pile base.	$q_{b,ult} = 8.5 p_A \left(\frac{q_{cb,avg}}{p_A}\right)^{0.5}$	The method is intended to predict the pile bearing capacity measured about 10 days after driving.

Source: Modified after Han, Prezzi, Salgado, & Zaheer, 2017.

Note: ϕ_c = critical-state friction angle; σ'_{h0} = initial horizontal effective stress at the depth being considered; B = pile diameter; R = pile radius; p_A = reference stress = 100 kPa = 1 tsf; q_c = representative cone resistance of the soil layer; σ'_{v0} = initial vertical effective stress at the depth being considered; δ_c = interface friction angle [ICP and UWA suggest using interface shear tests to determine the value of δ_c; if not feasible, it can also be estimated from the mean particle size (Jardine et al., 2005; Lehane et al., 2005b). δ_c can also be determined from the critical-state friction angle in sand by: $\delta_c = 0.9\phi_c$ (Foye, Abou-Jaoude, Prezzi, & Salgado, 2009; Salgado et al., 2011)]; $q_{cb,avg}$ = representative cone resistance at the pile base level; this can be obtained by averaging the cone resistances near the pile base level.

explained by the unrealistically high q_c measured near the pile base ($\approx$29 MPa = 4206 psi). As the pile base rests in a soil layer with high gravel content (50%), the overestimation of q_c appears to be an outcome of the relative size of the CPT cone compared with the gravels. Based on the theoretical equivalence of q_{bL} and q_c, the

TABLE 4.3
Values of the design parameters used in the capacity calculations

Depth (m)	Depth (ft)	γ_t[1] (kN/m^3)	γ_t[1] (lb/ft^3)	D_{50} (mm)	D_{50} (inch)	Gravel content (%)	ϕ_{cs} (°)	δ_{cs}/ϕ_{cs}	δ_{cs} (°)
0–5.5	18–8	19.5	125	—	—	0	30	0.82	24.6
5.5–8.2	18–27	20.0	128	0.4	0.02	4	32	0.82	26.2
8.2–10.4	27–34	21.5	138	4.5	0.18	49	35	0.66	23.1
10.4–16.8	34–55	20.0	128	0.9	0.04	10	32	0.76	24.3
16.8–22.6	55–74	21.5	138	4.1	0.16	43	34	0.68	23.1

Source: Modified after Ganju et al., 2018.
[1]Total unit weight.

TABLE 4.4
Shaft and base capacities measured from SLT and PDA and the pile capacities estimated from pile design methods at ultimate state (w/B = 10%)

Source	Method	Time after initial driving (days)	Shaft capacity (kips)	Base capacity (kips)	Total capacity (kips)
Predicted	Purdue-CPT	—	635	978	1,613
	ICP	10	462	813	1,276
	UWA	10–20	590	1,130	1,720
	NGI	—	824	858	1,681
	Fugro	10	712	945	1,657
Measured	PDA-EOID[1]	0	211	280	491
	PDA-BOR[1]	22	263	275	538
	SLT[2]	13	537	488	1,025
	SLT[3]	13	485	540	1,025

Source: Modified after Ganju et al., 2018.
[1]PDA results obtained from GRL.
[2]SLT results with shaft and base resistances not corrected for residual loads.
[3]SLT results with shaft and base resistances corrected for residual loads.

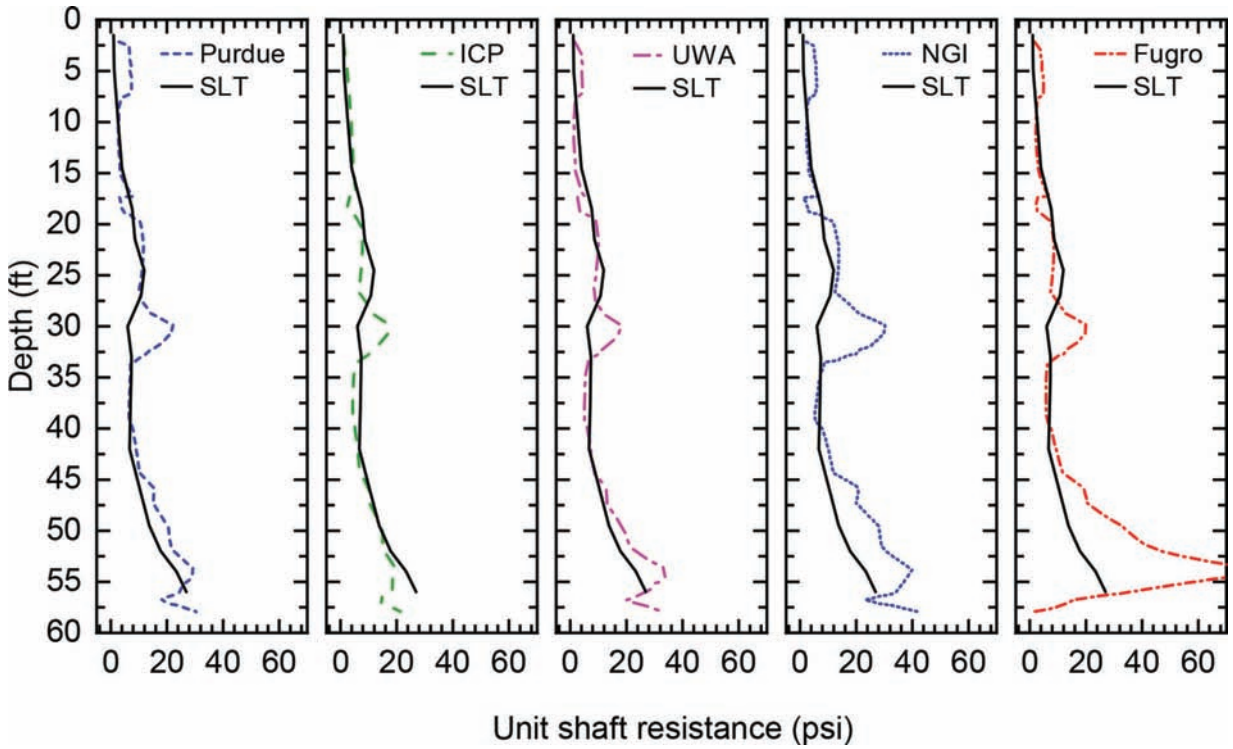

Figure 4.9 Comparison of unit shaft friction obtained from the SLT with estimates from CPT-based pile design methods. (Modified after Ganju et al., 2018.)

TABLE 4.5
The ratio of $q_{b,ult}$ to $q_{cb,avg}$ obtained from SLT and design methods at $w/B = 0.1$

Method	$q_{b,ult}/q_{cb,avg}$
SLT	0.29
Purdue	0.52
ICP	0.43
UWA	0.60
NGI	0.46
Fugro	0.50

Source: Modified after Ganju et al., 2018.

TABLE 4.6
The ratio of $q_{b,ult}$ to q_{bL} (assumed to be $q_{cb,avg}$) obtained from SLT and design methods at $w/B = 0.1$

Method	$q_{b,ult}/q_{bL}$
SLT	0.79
Purdue	0.77
ICP	0.43
UWA	0.60
NGI	0.66
Fugro	0.83

Source: Modified after Ganju et al., 2018.

ratio of base resistance at the ultimate limit state may be recalculated assuming q_c at the pile base to be equal to q_{bL}. This results in the measured $q_{b,ult}/q_c$ to be equal to 0.79. The $q_{b,ult}$ calculated from CPT design methods, using the $q_{cb,avg} = q_{bL}$ is presented in Table 4.6. The values appear to be closer to the measured ratio, suggesting that further work needs to be done to refine the current design methods under such conditions.

5. STATIC AND DYNAMIC LOAD TESTS OF THE OPEN-ENDED PIPE PILE

5.1 Pile Installation

Since the planed elevation for the head of the production piles was at a depth of 8.53 m (28 ft) below the ground surface, it was decided that the shaft resistance that would develop within this depth should not be measured in the static load test. To achieve this goal, a 0.91-m-diameter (36 inch) casing was driven to 8.53 m (28 ft), and the soil inside it excavated prior to pile driving (see Figure 5.1). The excavation may lead to local disturbance in soil near the bottom of the casing, but it would not affect the stress states in soil away from the bottom of the excavation as only a small cylindrical volume of soil was removed. As the surface roughness of pile plays an important role in the sand-pile interface behavior (Han, Ganju et al., 2018; Tehrani et al. 2016; Tehrani, Han, Salgado, & Prezzi, 2017), the roughness of the pile surfaces was measured by using a Mitutoyo SJ-410 profilometer. The average roughness Ra was in the range of 14–18 μm for the outer surface of the pile segments and in the range of 4–8 μm for the inner surface of the pile segments.

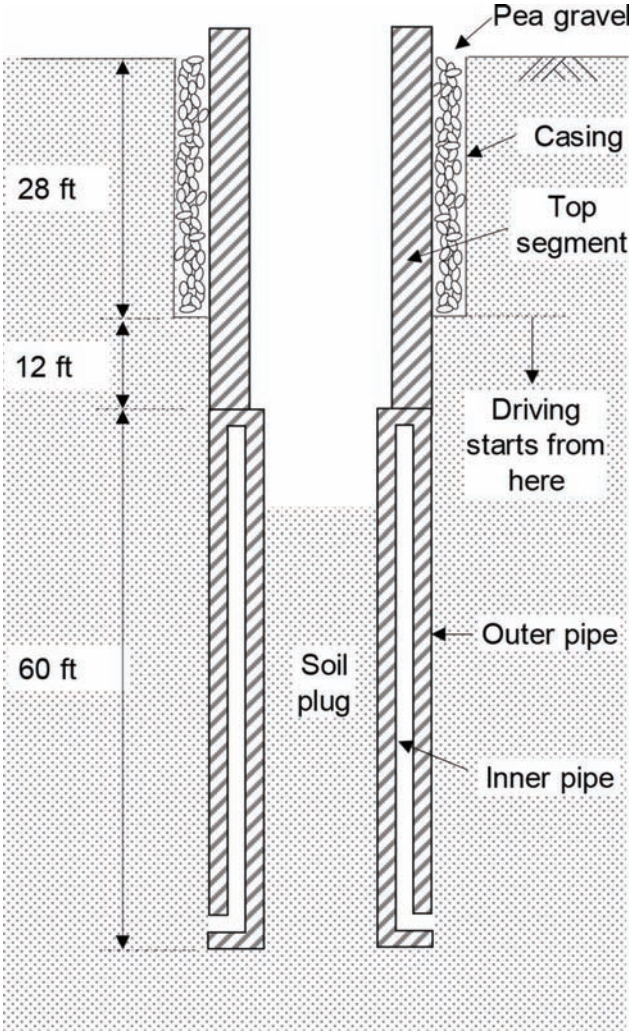

Figure 5.1 Dimensions of the test pile segments and schematics of the pile driving. (Modified after Han, Ganju, Prezzi, Salgado, & Zaheer, 2019.)

On October 1 and 4, 2016, the two segments of the test pile were driven in sequence by an APE Model D70-52 single-acting diesel hammer with a ram weight of 68.7 kN (15.4 kips) and a maximum stroke height of 3.43 m (11.25 ft), producing a maximum rated energy of 235.64 kN-m (173.64 ft-kips). Before the bottom segment was driven, the four centering bolts (shown in Figure 3.6c) welded near the tip of the segment were removed, and the holes left on the outer pipe were filled in by welding to prevent soil from entering the space between the two pipes during driving. Then, the bottom pile segment was lowered into the borehole, centered and driven into the ground to a depth of 16.8 m (55 ft) from the ground surface. After the top segment was positioned and welded to the bottom segment, the gauge cables from the bottom segment were joined with those from the top segment, fastened to the nuts welded along the two sides of the top segment, and protected with steel angles welded over the cables and strain gauges on the top. Considering the significant amount

of heat generated from welding, the gauge cables were wrapped with a thick layer of mineral wool for heat isolation. Three days after the driving of the bottom segment, the top segment was driven into the ground, with the pile base reaching a final depth of 30.48 m (100 ft) from the ground surface. The static load test took place 8 days after the initial driving, and a restrike was performed 7 days after that. The redundant part of the top segment was cut so that there was a 0.76-m-long (2.5 ft) segment of the pile exposed outside the ground surface for the static load test. Figure 5.1 shows the dimensions of the pile segments. After pile driving, loose pea gravel was used to backfill the gap between the casing and the test pile to prevent lateral instability during the static load test.

Figure 5.2 shows the blow counts per meter of penetration recorded during pile driving. The driving resistance increased almost linearly with penetration depth. Pile driving started with the pile base placed (inside the pre-drilled borehole) at a depth of 8.53 m (28 ft), where the confining effective stress in the soil is not zero, thus resulting in about 40 blows/m in the beginning of driving. This is different from the normal cases in which piles are driven from the ground surface, in which case blow counts at the beginning of driving are nearly zero (Han, Prezzi, Salgado, & Zaheer, 2017; Paik et al., 2003). No discontinuity was observed in the profile of blow counts for the installation of the top and bottom pile segments, suggesting that no set-up was developed for the bottom pile segment during the three-day wait period between driving of the two segments. Plug measurement following the scheme discussed in the previous section was carried out throughout the pile driving process. Figure 5.3 plots the length of the plug that formed inside the open-ended pile as the pile was driven into the ground. The calculated IFR decreased from 92% at the beginning of driving to 70% at the end of driving, when the final PLR was 77.7%. Dynamic load (PDA) tests were performed by GRL Engineers, Inc. at the end of the initial pile driving (EOID) and at the beginning of the restrike (BOR) on October 19, 2016, 15 days after the initial driving. The pile resistances obtained from the PDAs are summarized in Table 5.1.

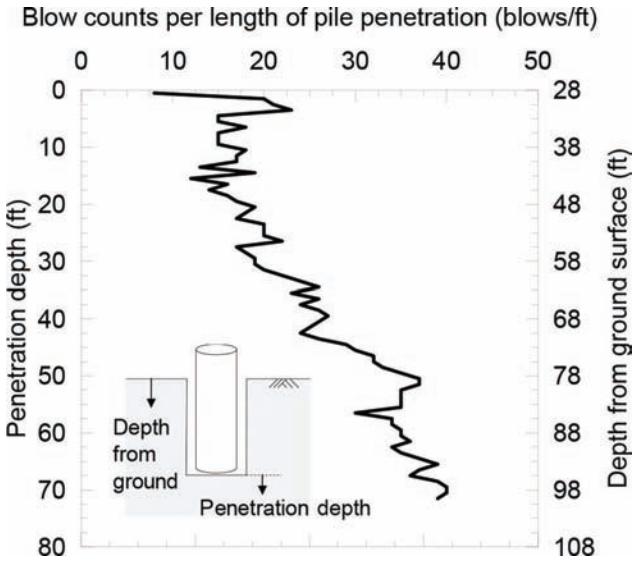

Figure 5.2 Blow counts during pile driving. (Modified after Han, Ganju, Prezzi, Salgado, & Zaheer, 2019.)

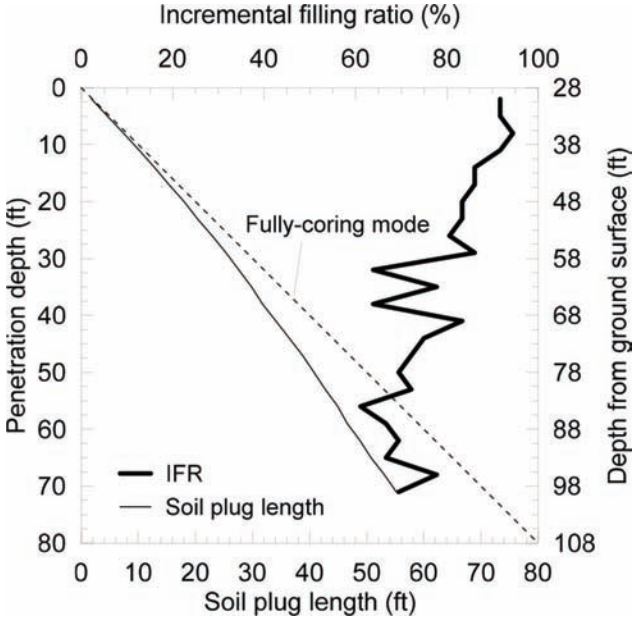

Figure 5.3 Plug measurements during pile driving: soil plug length and the incremental filling ratio. (Modified after Han, Ganju, Prezzi, Salgado, & Zaheer, 2019.)

5.2 Static Pile Load Test

Figure 5.4 shows the loading system assembled for load application and force and displacement measurement during the static load test. The axial load was applied by a hydraulic jack (20 MN, AFT-cell® Model 24) placed between the pile cap and the load cell, which transferred the load to the reaction beam through the spherical seating. The magnitude of the applied load was measured by a load cell calibrated shortly before the load test. Load cell measurements were cross-checked by the pressure gauge readings in the hydraulic jack, which had been calibrated separately from the load cell. Four electrical dial gauges, placed 90 degrees apart from each other, were mounted on reference beams to measure the pile head settlements at these four locations. All parts of the loading system were carefully aligned to ensure that the static load was applied through the center of the pile and that no bending moment was introduced due to eccentric loading to the extent that that can be done in the field. This was reflected in the maximum differential settlement at the pile head measured by the four dial gauges, which was only 0.56 mm (0.022 inch) at the end of loading, when the total average settlement at the pile head was 149 mm (5.87 inch).

TABLE 5.1
Resistances measured by different methods at different times

Source of capacities	Time after initial driving (days)	Shaft resistance (kips)	Plug resistance (kips)	Annulus resistance (kips)	Base resistance (plug resistance + annulus resistance) (kips)	Total resistance (kips)
PDA-EOID[1]	0	328	—	—	175	503
PDA-BOR[1]	15	236	—	—	305	541
Static load test[2]	8	576	80	419	499	1,075
Static load test[3]	8	509	70	496	566	1,075

Source: Modified after Han, Ganju, Prezzi, Salgado, & Zaheer, 2019.
[1]Obtained from PDAs performed by GRL Engineers, Inc.
[2]Without correction for residual loads.
[3]After correction for residual loads.

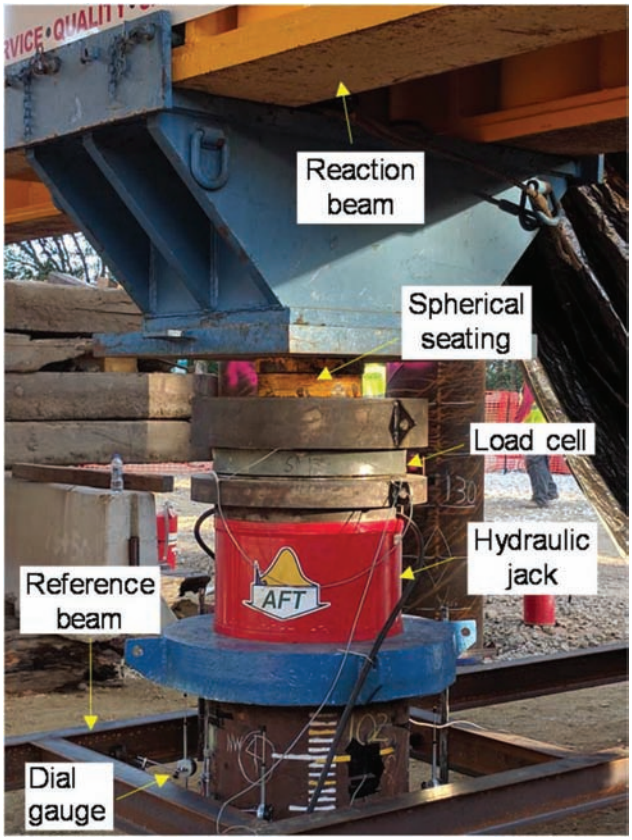

Figure 5.4 Setup of the loading system and settlement measurement for the static load test. (Modified after Han, Ganju, Prezzi, Salgado, & Zaheer, 2019.)

In order to obtain a complete, realistic and well-defined load-settlement curve, a slow-maintained static load test was performed with small load increments, in contrast to the four equal increments prescribed in ASTM (2013) or the eight equal increments prescribed in EUROCODE-7 (Selig, 1985). The static axial load test started on October 12, 2016 (8 days after pile driving). The pile was first loaded to 2225 kN (500 kips) with loading increments of 445 kN (100 kips). After that, smaller increments ranging from 222 kN (50 kips) to 111 kN (25 kips) were used until the end of the test. After each load increment was applied, the pile head settlement was recorded at zero, one, two, five, and ten minutes and every ten minutes thereafter. The load at each load step was maintained until the settlement rate at the pile head obtained from two consecutive settlement readings became equal or less than 0.25 mm/hr. In case this criterion could not be met in two hours, the next increment was added only after the difference between two consecutive settlement readings was less than 5%. At a load equal to 6228 kN (1400 kips), the pile started plunging into the ground with a settlement rate of 50 mm/hr. Loading was then terminated, and the pile was unloaded in four equal decrements with a waiting period of 15 min between each load decrement. The static load test lasted 40 hours.

During the static load test, two separate data acquisition (DAQ) systems were used to collect data from the two types of strain gauges due to their different principles of measurement. Geokon Model 8025 series Micro-800 Datalogger and one additional multiplexer (Geokon Model 8032) were used for the vibrating-wire strain gauges, whereas Campbell Scientific Model CR9000X Datalogger with a series of Analog Input Modules (Model CR9050 5-Volt) was used for the electrical-resistance strain gauges. The Model CR9000X Datalogger does not have Wheatstone bridges built in; thus, each electrical-resistance strain gauge was connected to the Datalogger through a 4WFBS350 (350 Ohm, 4-Wire, Full-Bridge) Terminal Input Module. Loggernet, a software developed by Campbell Scientific, was used to display and store data collected through the dataloggers. Readings were taken every 4 seconds for the electrical-resistance strain gauges and every 2 minutes for the vibrating-wire strain gauges.

5.3 Test Results

5.3.1 Load Settlement Curve

Figure 5.5a shows the load-settlement curve obtained from the static load test on the open-ended test pile. The square symbols in the figure represent intermediate readings that were used to determine the pile head

settlement rate at each load level during the static load test. The total resistance for an open-ended pile is the summation of three resistance components: shaft, plug, and annulus resistances. These, calculated from the strain gauges, are shown in Figure 5.5b.

When the test pile was loaded, the rate of total resistance mobilization with respect to pile head settlement was quite high, dropping fast to a load level of 2,224 kN (500 kips), which corresponded to a pile head settlement of 9 mm (= 0.0136*B*). After that, the total resistance continued to increase with a much gentler slope; this is because the majority of the shaft resistance had already been mobilized at that stage, as shown in Figure 5.5b, and additional load applied at the pile head was taken mainly by the pile base. The annulus resistance mobilization started almost immediately upon load application; in contrast, plug resistance increased very slowly initially, building up more significantly only when the pile head settlement reached 30 mm (1.18 inch) (= 0.045*B*). Plug mechanics involves a plug base load applied by the soil below the pile base and the counter-balancing shear force that develops between the plug and the inner surface of the pile (Randolph, 2003). If the pile advances with a relatively small plug base load, there will be minimal compression of the lower end of the plug, mobilizing a small inner shaft resistance near the pile base. As loading proceeds and the plug densifies, these opposing forces become more significant and the plug resistance builds up.

The ultimate pile resistance has been widely defined as the resistance developed when the pile head settlement equals 10% of the pile diameter *B*; most current design methods associate the estimated pile bearing capacity with a pile head settlement equal to 0.1*B* (Basu & Salgado, 2014; Clausen et al., 2005; Han, Lim, Salgado, Prezzi, M, & Zaheer, 2015; Han, Salgado, Prezzi, & Lim, 2017; Han, Prezzi, & Salgado, 2018; Han, Salgado, & Prezzi, 2018; Jardine et al., 2005; Kolk et al., 2005; Lehane et al., 2005b; Randolph, 2003; Salgado, Han, & Prezzi, 2017). The ultimate resistance of the test pile, corresponding to a pile head settlement of 66 mm (2.69 inch) (= 0.1*B*), was 4782 kN (1075 kips). A pile head settlement of 149 mm (5.87 inch) (= 0.225*B*) was required for the pile to start plunging into the ground.

5.3.2 Residual Loads

Immediately after the end of pile driving, the compressed soil below the pile base tends to rebound, pushing the pile upwards, while the pile tends to recover the elastic deformation caused by driving. Pile displacement is resisted by the surrounding soil, leading to non-zero residual loads locked in the pile (Briaud & Tucker, 1984; Fellenius et al., 2004; Han, Prezzi, Salgado, & Zaheer, 2017; Kim et al., 2009; Lee et al., 2003; Paik et al., 2003; Poulos, 1987; Seo et al., 2009).

As indicated earlier, due to the inertial force during the pile driving process, even a small slippage between a vibrating rod and the mounting blocks (Figure 3.3a) may induce a drift in the reading of a vibrating-wire strain gauge, making it not suited to estimating residual loads. In contrast, the lightweight electrical-resistance strain gauges are not affected by inertial forces. Therefore, they are more suitable for the measurement

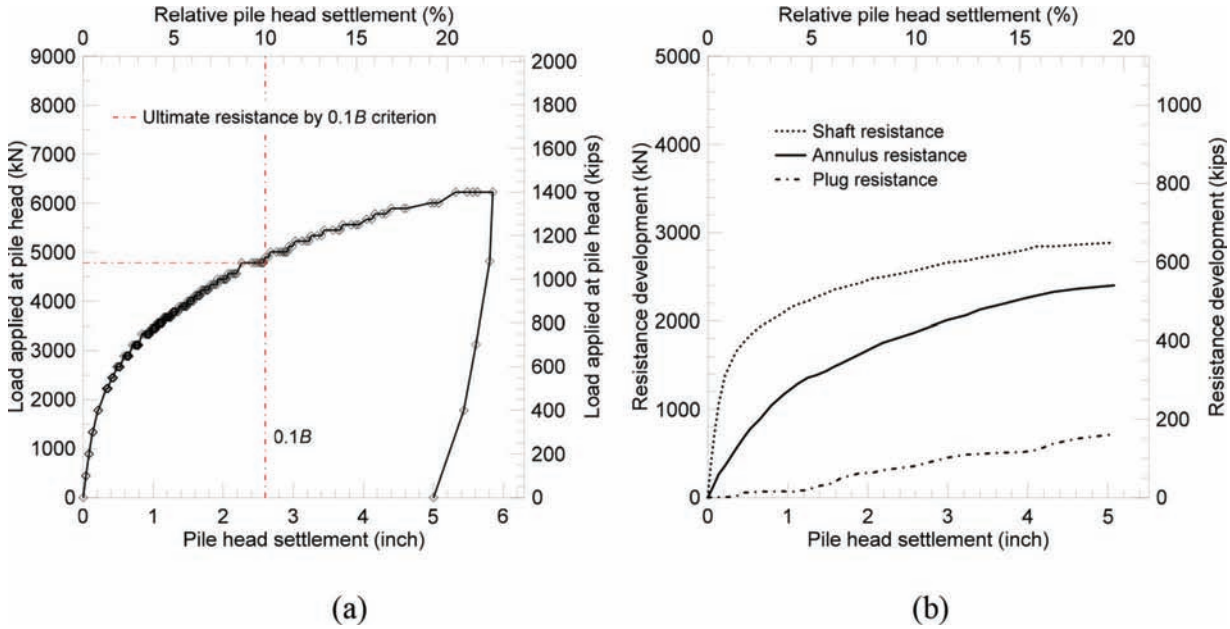

Figure 5.5 Load-settlement response during the static load test: (a) load-settlement curve (including intermediate readings, taken during each load step); (b) mobilization of the shaft, plug and annulus resistances during the static load test. (Modified after Han, Ganju, Prezzi, Salgado, & Zaheer, 2019.)

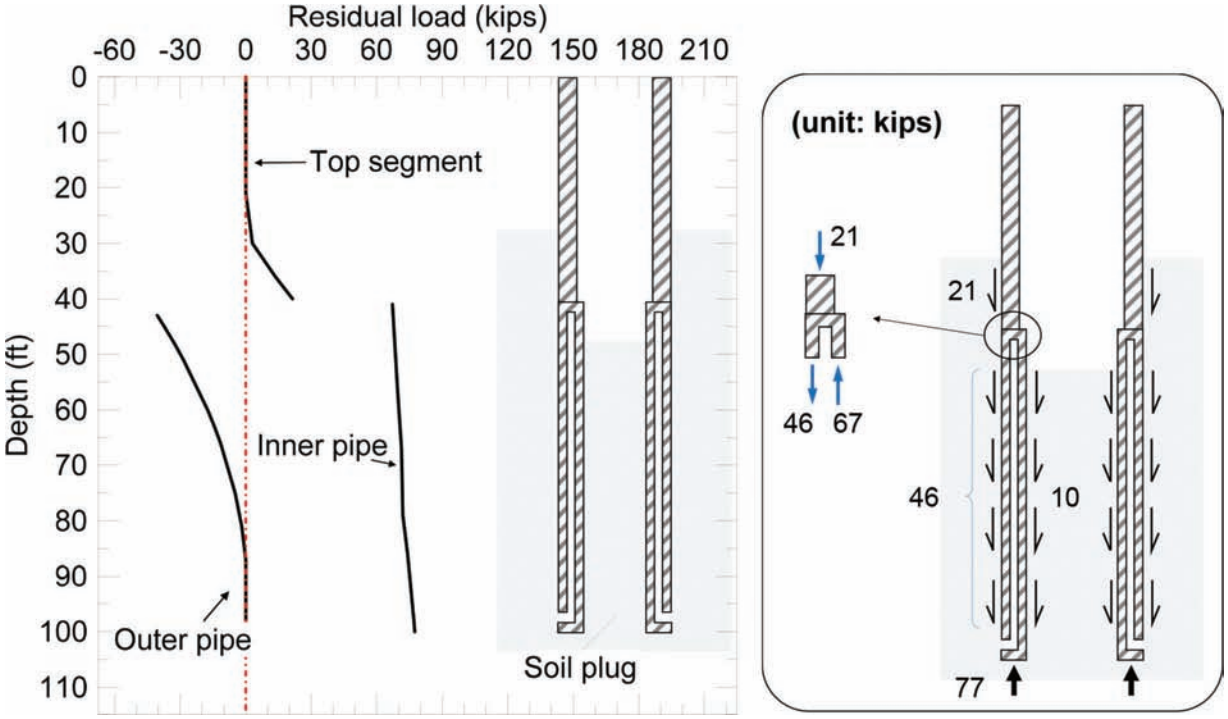

Figure 5.6 Profile of measured residual loads in all pile segments and the force balance for the pile segments. (Modified after Han, Ganju, Prezzi, Salgado, & Zaheer, 2019.)

of residual loads (Hajduk & Paikowsky, 2000; Han, Prezzi, Salgado, & Zaheer, 2017).

All electrical-resistance strain gauges were zeroed before pile driving so that the locked-in residual load could be obtained from the strain gauge readings collected at the end of driving. Figure 5.6 shows the measured residual loads in each segment of the test pile. The residual load in the top segment and the inner pipe was compressive, whereas the residual load in the outer pipe was tensile. Since the head of the pile was free, and the top 8.53 m (28 ft) of the pile (inside the casing) was not in contact with soil at the end of driving, the residual load in the top 8.53 m (28 ft) of the pile was zero. Figure 5.6 also shows the force balance for the pile segments. At the end of driving, there was a compressive force of 342 kN (77 kips) on the annulus of the inner pipe. This force was balanced by the shaft resistances acting (downwards) on the inner pipe (44 kN = 10 kips) and on the outer pipe (298 kN = 67 kips).

5.3.3 Shaft and Base Resistances

When the static load was applied at the head of the open-ended test pile, the load was transferred from the top single-pipe segment to the bottom double-wall segment. The load distribution within the pile can be obtained from the strain gauge readings. Figure 5.7a shows the load transfer curves at the ultimate load level with no residual load correction. The load decreases with increasing depth, as the load applied at the head of the pile is gradually transferred to the surrounding soil through frictional resistance along the pile shaft.

Since all strain gauges were re-zeroed before the static load test, the measurements during the test were in addition to the locked-in residual loads that already existed in the pile (due to pile installation) before the test. Thus, the actual loads in the pile are the summation of the locked-in residual loads and the loads directly measured during the static load test. Figure 5.7b shows the load transfer curves after correction for the residual loads. The values of all the resistance components with and without correction for the residual loads are summarized in Table 5.1.

Figure 5.8 shows the profiles of the unit shaft resistance at the ultimate load level with and without correction for the residual loads. As seen in many other pile load tests (Han, Prezzi, Salgado, & Zaheer, 2017; Paik et al., 2003), the unit shaft resistance is generally less after correction for residual loads. This is because the residual shaft resistance for most of the pile length, if not over the entire length of the pile, points downwards to resist the upward movement of the pile during the rebound at the end of driving.

In empirical pile design methods, the unit shaft resistance is often directly related to the initial vertical effective stress σ'_{v0} by: $q_{sL} = \beta\sigma'_{v0}$; this is known as the β method. Figure 5.9 shows the back-calculated β values ($= q_{sL}/\sigma'_{v0}$) for the outer surface of the test pile

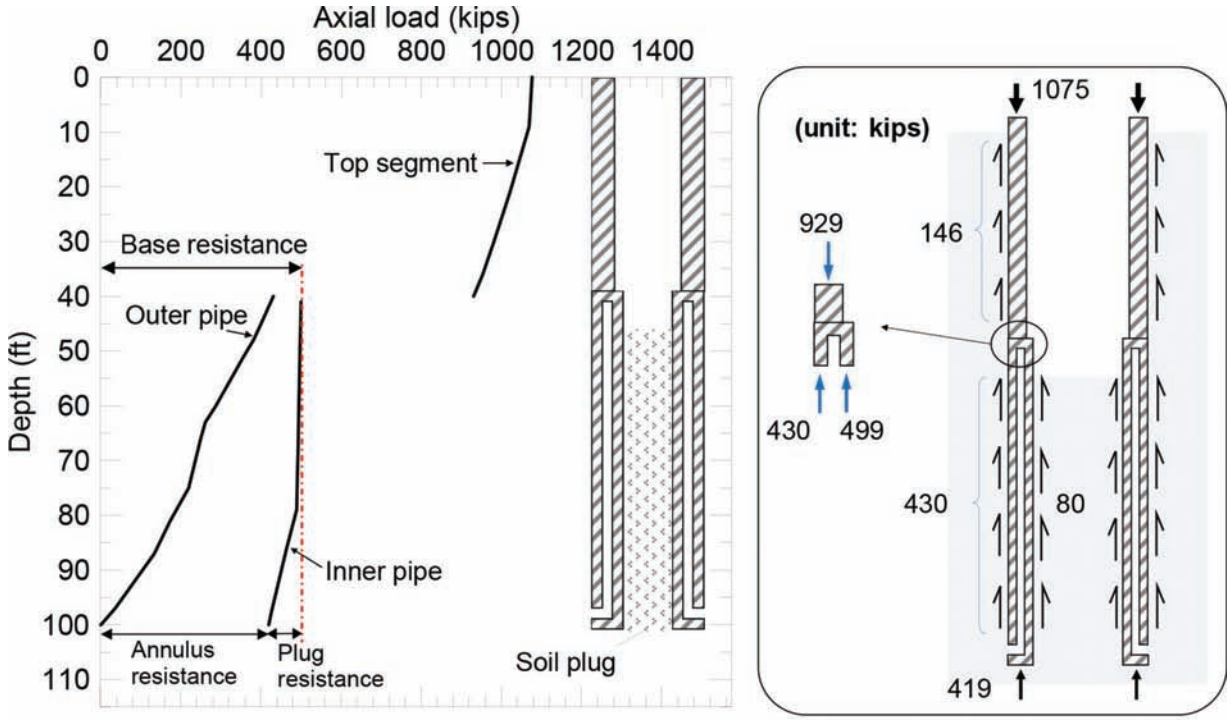

(a)

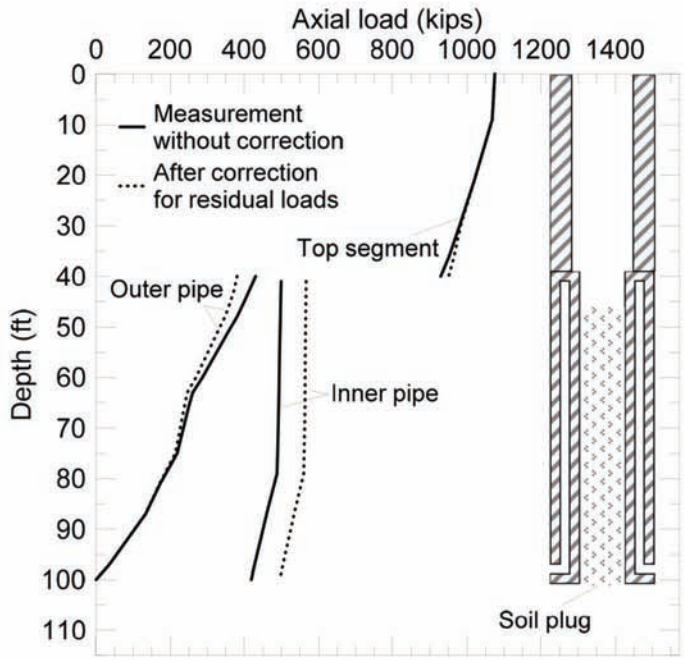

(b)

Figure 5.7 Load transfer curves at the ultimate load level ($w = 0.1B$): (a) without correction for the residual loads; (b) after correction for the residual loads. (Modified after Han, Ganju, Prezzi, Salgado, & Zaheer, 2019.)

at the ultimate load level after correction for the residual loads. The limit unit shaft resistance can also be considered as a fraction of the cone resistance q_c in design practice. The ratio between q_{sL} and q_c is shown in Figure 5.9. The ratio obtained from the static load test is in a similar range (0.15%–0.4%) as that suggested by Lee et al. (2003) for open-ended pipe piles. Given the frictional nature of the unit limit shaft resistance, it can also be expressed as the product of the mobilized normal effective stress σ'_h and the tangent of the pile-soil interface friction angle δ_{cs} at the critical state: $\sigma'_h \tan\delta_{cs}$, and $\sigma'_h = K\,\sigma'_{v0}$, where K is the mobilized coefficient of lateral earth pressure and σ'_{v0} is the initial *in-situ* vertical effective stress at the depth being considered. The profile of K obtained from the static load test is plotted in Figure 5.9 along with other quantities of interest.

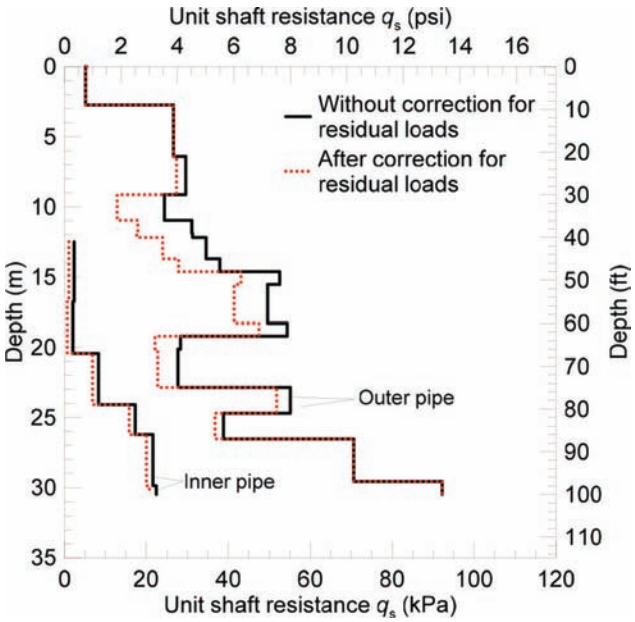

Figure 5.8 Profiles of the unit shaft resistance on the outer and inner pipes at the ultimate load level ($w = 0.1B$) with and without correction for the residual loads. (Modified after Han, Ganju, Prezzi, Salgado, & Zaheer, 2019.)

The unit annulus resistance q_{ann} and the unit plug resistance q_{plug} can both be related to a representative cone resistance $q_{cb,avg}$ at the pile base. Table 5.2 summarizes the values of q_{ann} and q_{plug} normalized with respect to $q_{cb,avg}$ (= 22.8 MPa = 3307 psi) at several settlement levels. Because the diameter of the cone used in the CPT test, 44.45 mm (1.75 inch), is comparable in size to the wall thickness (50.8 mm = 2 inch) of the test pile, the unit annulus resistance q_{ann} is comparable in magnitude to the cone resistance $q_{cb,avg}$ at the ultimate load level.

The soil plug was inactive at the beginning of loading, with q_{plug} mobilized only to $0.01q_{cb,avg}$ when $w = 0.05B$. As the loading progressed further, the soil plug gradually became active, and a plug resistance $q_{plug} = 0.06\ q_{cb,avg}$ was measured at the ultimate load level ($w = 0.1B$), with this value then doubled (= $0.12\ q_{cb,avg}$) at the plunging load. This would suggest that the proposal of Lehane and Randolph (2003) of considering plug resistance to be comparable to the values of base resistance for non-displacement piles, calculated using the Lee and Salgado (1999) q_b/q_c relationships, which works well in sand, might slightly overpredict plug resistance in gravelly sand because of the high q_c values.

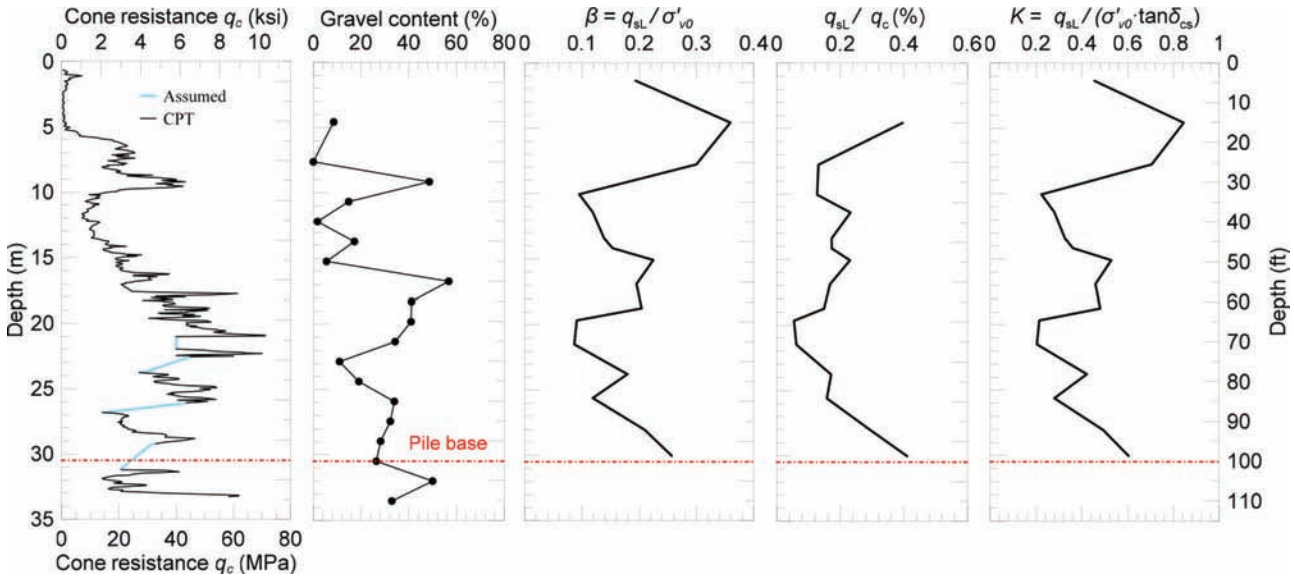

Figure 5.9 Cone resistance, gravel content, $\beta\,(= q_{sL}/\sigma'_{v0})$, normalized unit limit shaft resistance q_{sL}/q_c and coefficient of lateral earth pressure $K\,(= q_{sL}/(\sigma'_{v0}\tan\delta_{cs}))$ along the test pile after correction for the residual loads. (Modified after Han, Ganju, Prezzi, Salgado, & Zaheer, 2019.)

5.4 Design Methods for Open-Ended Pipe Piles

Design methods have been proposed to estimate the bearing capacity of open-ended pipe piles driven in sand. In absence of well-developed design methods for open-ended piles in gravelly soil, two of the sand methods, ICP and UWA methods, were used to estimate the axial capacity of the test pile. Table 5.3 summarizes the design equations for these methods, and Table 5.4 provides the input values of the parameters used in the estimations. As seen in Figure 5.10, the profile of the CPT cone resistance has sharp peaks and valleys because of the gravel particles present in the soil profile. Given that the cone is not substantially greater than the gravel particles, the cone resistance in soil with a large gravel content reflects the response of soil that should be viewed not as a continuum but as a discrete particulate system. When the advancing cone hits a large particle, it pushes it down with it, and the cone resistance reflects the resistance to penetration not only of the cone but also of a larger object, which may, in addition, hit against and even interlock with other large particles, leading to peaks in the cone resistance profile. When the cone then

TABLE 5.2
Annulus resistance and plug resistance (after correction for residual loads) normalized with respect to cone resistance $q_{cb,avg}$ at the pile base at different relative settlement levels

Relative pile head settlement w/B	Annulus resistance Q_{ann} (kips)	Unit annulus resistance q_{ann} (MPa)	$q_{ann}/q_{cb,avg}$	Plug resistance Q_{plug} (kips)	Unit plug resistance q_{plug} (MPa)	$q_{plug}/q_{cb,avg}$
0.05	386	16.5	0.72	13	0.2	0.01
0.1 (ultimate load)	496	21.2	0.93	70	1.3	0.06
0.225 (plunging load)	616	26.3	1.15	152	2.8	0.12

Source: Modified after Han, Ganju, Prezzi, Salgado, & Zaheer, 2019.

TABLE 5.3
Design methods used for the estimation of the pile resistances for open-ended pipe piles in sand

Method and key reference	Limit unit shaft resistance q_{sL}	Ultimate unit base resistance $q_{b,ult}$	Comments
ICP (Jardine et al., 2005)	$q_{sL} = \left(\sigma'_{rc} + \Delta\sigma'_{rd}\right) \tan\delta_{cs}$ $\sigma'_{rc} = 0.029 q_c \left(\frac{\sigma'_{v0}}{p_A}\right)^{0.13} \left(\frac{h}{R^*}\right)^{-0.38}$, $R^* = \left(R^2 - R_i^2\right)^{0.5}$ $\Delta\sigma'_{rd} = 2G\Delta r / R$ $G = q_c \left[0.0203 + 0.00125\eta - 1.216\times10^{-6}\eta^2\right]^{-1}$ $\eta = q_c \left(p_A\, \sigma'_{v0}\right)^{-0.5}$ R^* is equivalent radius; Δr = 0.02 mm for lightly rusted steel piles; h is the distance from the depth being considered to the pile base, $h/R^* \geq 8$.	Pile is unplugged if: $B_i \geq 0.02(D_R - 30)$ *or* $\frac{B_i}{B_{CPT}} \geq 0.083 \frac{q_c}{P_A}$ Unplugged: $q_{b,ult} = q_c$ (on the annular area) Plugged: $q_{b,ult} = \max[0.5\text{–}0.25 \log(B/B_{CPT}),\ 0.15,\ A_r] q_{cb,avg}$ D_R is relative density, in percentage; B_{CPT} is cone diameter (= 0.0445 m in the present case).	Intended to predict the pile bearing capacity 10 days after driving for "virgin" piles.
UWA (Lehane et al., 2005b)	$q_{sL} = \frac{f}{f_c}\left(\sigma'_{rc} + \frac{4G\Delta r}{B}\right) \tan\delta_{cs}$ $\sigma'_{rc} = 0.03 \cdot q_c (A_{rb}{}^*)^{0.3} \left[\max\left(\frac{h}{B}, 2\right)\right]^{-0.5}$, $A_{rb}{}^* = 1 - \mathrm{IFR}\left(\frac{B_i}{B}\right)^2$ $G/q_c = 185 \left[\frac{q_c/p_A}{\left(\sigma'_{v0}/p_A\right)^{0.5}}\right]^{-0.75}$ $\Delta r = 0.02$ mm f/f_c = 1 for compression and 0.75 for tension; $A_{rb}{}^*$ is effective area ratio; IFR is incremental filling ratio, $\mathrm{IFR}_{mean} \approx \min[1, (B_i/1.5)^{0.2}]$, B_i in meters.	$q_{b,ult} = (0.15 + 0.45\, A_{rb}{}^*) q_{cb,avg}$ $A_{rb}{}^* = 1 - \mathrm{FFR}\left(\frac{B_i}{B}\right)^2$ FFR is final filling ratio measured at the end of pile driving, average over $3B_i$, if not measured, it can be roughly approximated by using the same equation of IFR.	The method is intended to predict the pile bearing capacity measured 10–20 days after driving.

Source: Modified after Han, Ganju, Prezzi, Salgado, & Zaheer, 2019.

Note: ϕ_{cs} is the critical-state friction angle; σ'_{h0} is the initial horizontal effective stress at the depth being considered; B is the pile outer diameter; B_i is the pile inner diameter; R is the outside pile radius; R_i is the inside pile radius; p_A is the reference stress = 100 kPa; q_c is the representative cone resistance of the soil layer; σ'_{v0} is the initial vertical effective stress at the depth being considered; δ_{cs} is the interface friction angle [ICP and UWA suggest using interface shear tests to determine the value of δ_{cs}; if not feasible, it can also be estimated from the mean particle size (Jardine et al., 2005; Lehane et al., 2005b); $q_{cb,avg}$ is the representative cone resistance at the pile base level; this can be obtained by averaging the cone resistances near the pile base level.

finally pushes the large particle aside, a valley may be observed in the cone resistance profile, which, depending on the gravel content, may be more representative of composite action of the matrix soil and gravel.

In our calculations, values of cone resistance from a lower-bound profile drawn approximately through the valleys of the profile were used to estimate the shaft resistance of the test pile. Figure 5.10 compares the unit limit shaft resistance profiles obtained from the static load test and the ICP and UWA design methods. The two methods produce good estimates above z = 16 m (52 ft), where the soil has a lower gravel content, except for a thin layer between z = 8 m (26 ft) to 9 m (30 ft). Both design methods significantly overestimate the unit shaft resistance below z = 16 m (52 ft), where the gravel content was greater than 30% at most depths.

Table 5.5 compares the shaft and base resistances measured from the static load test with the estimates obtained by using the ICP and UWA methods. While these sand methods overestimate the shaft resistance by a factor of two, they produce good estimates for the base resistance. This is because the annulus resistance takes the main portion of the base resistance in the present case, and the annulus (wall) thickness is comparable to that of the CPT cone, and therefore the cone resistance obtained is representative of what the pile annulus would experience.

TABLE 5.4
Values of the design parameters used in the resistance calculations

Layer no.	Depth (m)	Depth (ft)	γ_t kN/m^3)	γ_t[1] (lb/ft^3)	D_{50} (mm)	D_{50} (inch)	Gravel content	ϕ_{cs} (deg)	δ_{cs}/ϕ_{cs}	δ_{cs} (deg)
1	0–5.5	0–18	19.5	125	—	—	0%	30	0.82	24.6
2	5.5–8.2	18–27	20.0	128	0.4	0.02	4%	32	0.82	26.2
3	8.2–10.4	27–34	21.5	138	4.5	0.18	49%	35	0.66	23.1
4	10.4–16.8	34–55	20.0	128	0.9	0.04	10%	32	0.76	24.3
5	16.8–22.6	55–74	21.5	138	4.1	0.16	43%	34	0.68	23.1
6	22.6–32.6	74–107	21.5	138	1.1	0.04	28%	33	0.76	25.1

Source: Modified after Han, Ganju, Prezzi, Salgado, & Zaheer, 2019.

Note: The critical-state internal friction angle ϕ_{cs} was estimated from the mean particle size D_{50}, based on the dependence of ϕ_{cs} on D_{50} observed by Han et al. (2018). The ratio δ_{cs}/ϕ_{cs} was evaluated based on the relationship proposed by Han et al. (2018) between δ_{cs}/ϕ_{cs}, D_{50}, and pile surface condition (rusted steel in the current case).

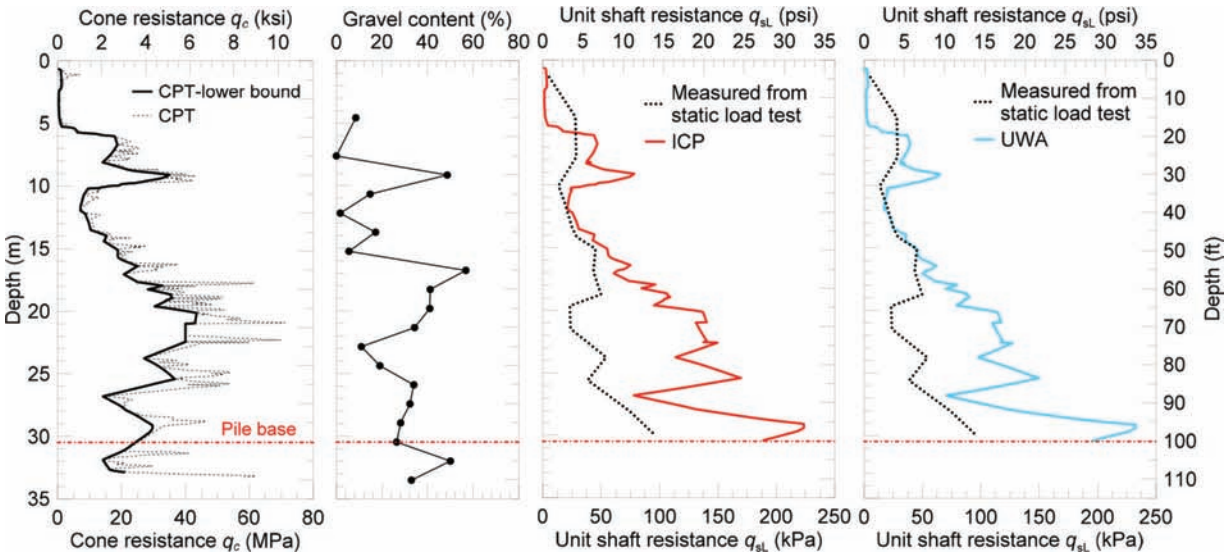

Figure 5.10 Cone resistance qc, gravel content, and comparison of the unit limit shaft resistance q_{sL} obtained from the static load test (after correction for the residual loads) and those estimated by using the ICP and UWA methods. (Modified after Han, Ganju, Prezzi, Salgado, & Zaheer, 2019.)

TABLE 5.5
Comparison between the predicted and measured (at the ultimate load level when $w = 0.1B$) pile capacities

Source of capacities	Time after initial driving (days)	Shaft resistance (kips)	Plug resistance (kips)	Annulus resistance (kips)	Base resistance (plug resistance + annulus resistance) (kips)	Total resistance (kips)
Static load test[1]	8	576	80	419	499	1,075
Static load test[2]	8	509	70	496	566	1,075
ICP method	10[3]	1,084	—	—	499	1,582
UWA method	10[3]	958	—	—	589	1,547

Source: Modified after Han, Ganju, Prezzi, Salgado, & Zaheer, 2019.
Note: values shown in bold are the experimental results to which the predictions are compared.
[1]Without correction for residual loads.
[2]After correction for residual loads.
[3]The time after pile installation to which the prediction method applies.

6. COMPARISON OF THE RESPONSE OF THE CLOSED- AND OPEN-ENDED PIPE PILES

6.1 Driving Resistance

As the test piles were driven into the ground, the blow counts per unit length of pile penetration were recorded for all the test and reaction piles. As shown in Figure 6.1, the driving resistance for the closed-ended test pile is always greater than that for the open-ended test pile (with almost the same outer diameter). The driving resistance records for the open-ended reaction piles (with layouts and dimensions provided in Figure 6.2) are plotted in Figure 6.3. The driving resistance of the open-ended test pile was greater than those of all the reactions piles because the annulus thickness (=2 inch) of the open-ended test pile was greater than that (=0.5 inch) of the reaction piles.

The length of the soil plugs of all the open-ended test piles was continuously measured during the entire driving process by using the aforementioned weight system and the measurement scale on the piles. Figure 6.3 shows the driving resistance records and the incremental filling ratio IFR plotted as a function of depth for all the open-ended pipe piles. The final plug ratio PLR for the open-ended test pile was 77.7% at the end of driving, when the IFR was 70%. Plug formation for the four reaction piles (ROEP 3, 6, 7, and 10 in Figure 6.2) was also measured, and the profiles of the IFR for these piles are compared with that of the test pile in Figure 6.3b. The IFR for the test pile was greater than those for the reaction piles at the beginning of driving, and as driving continued, the IFR of the test pile gradually approached that of the reaction piles. This is because the driving of the open-ended test pile started at a depth of 8.53 m (its plug length was zero at this depth). On the other hand, when the reaction piles (which were driven from the ground surface) reached a driving depth of 8.53 m, there was already a volume of soil (plug) inside the pile that resisted the soil below the pile from entering it. This resulted in a lower IFR than that of the test pile. As the lengths of the plugs of the test pile and the reaction piles increased, the values of the IFR became similar, as can be seen in Fig 6.3b.

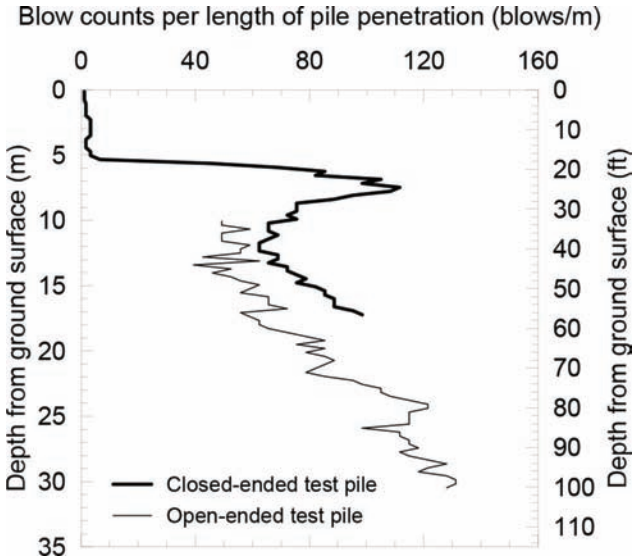

Figure 6.1 Comparison of the driving resistance (blow counts) of the closed-ended and open-ended test piles. (Modified after Han, Ganju, Salgado, & Prezzi, in press b.)

Despite the differences observed in the driving resistance records of the reaction piles, the profiles of the incremental filling ratio for these piles were similar and repeatable. This was caused by the gravel-size particles present in the soil profile. As the pile was driven into the ground, the driving resistance might increase or drop drastically as the pile annulus (13 mm (0.51 inch) in thickness for the reaction piles) encountered large particles (as large as 50 mm (1.97 inch)) or when these particles moved out of the way of the advancing pile. In contrast, plug formation is less affected by these local variations in gradation in the soil profile since it results mainly from the interaction of the entire soil plug with the surrounding pile inner surface and the soil right beneath the soil plug.

6.2 Load-Settlement Response

The limit and ultimate resistances of the piles were obtained from the load-settlement curves. The ultimate load was defined as the resistance developed when the pile head settlement $w = 0.1B$ (B being the pile outer

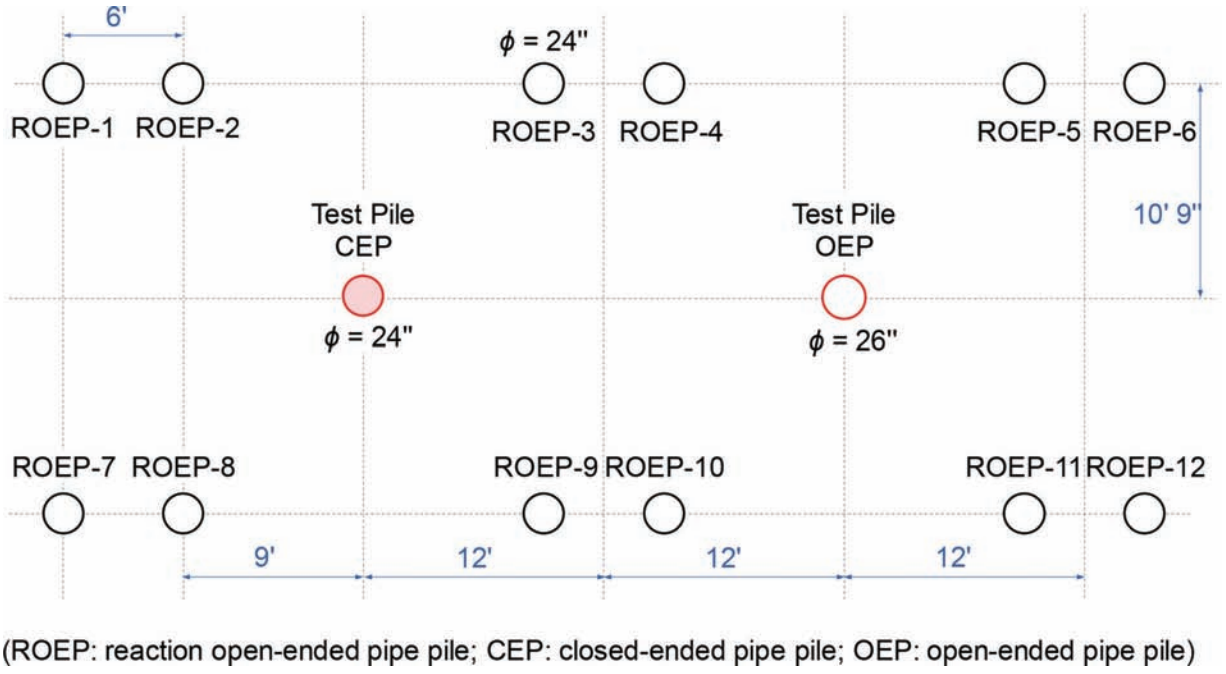

Figure 6.2 Layout of the two test piles and the reactions piles for the static load tests. (Modified after Han, Ganju, Salgado, & Prezzi, in press b.)

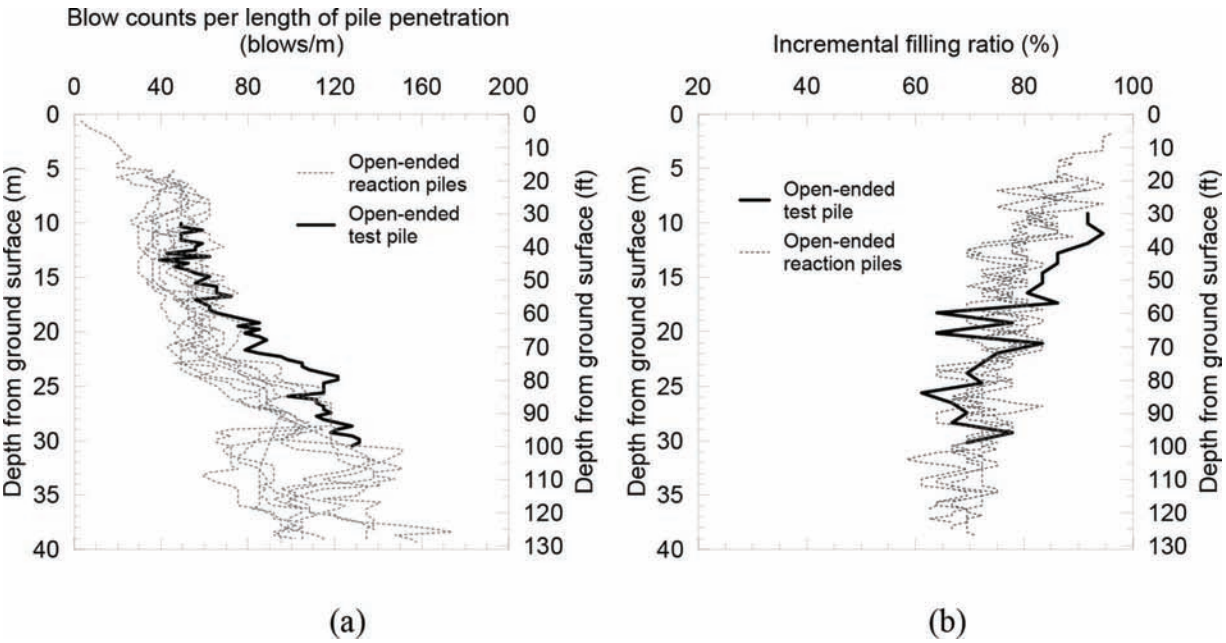

Figure 6.3 Driving records of the open-ended test pile and the open-ended reaction piles: (a) blow counts; (b) incremental filling ratio (IFR) measured during pile driving. (Modified after Han, Ganju, Salgado, & Prezzi, in press b.)

diameter in the case of the open-ended pipe pile). The $0.1B$ ultimate load criterion is widely used, and most of the current pile design methods predict pile resistances defined according to this criterion (Basu & Salgado, 2014; Clausen et al., 2005; Gavin & Lehane, 2007; Han, Prezzi, Salgado, & Zaheer, 2017; Han, Salgado, Prezzi, & Lim, 2017; Jardine et al., 2005; Kolk et al., 2005; Lehane et al., 2005b; Randolph, 2003; Xu, Schneider, & Lehane, 2008)

Figure 6.4 shows the load-settlement curves obtained from the static load tests for the two test piles. By using the $0.1B$ criterion, the ultimate resistances were determined as 4,559 kN (1,025 kips) for the closed-ended test pile and 4,782 kN (1,075 kips) for the open-ended test pile. The open-ended test pile showed greater additional resistance mobilization from the ultimate load to the plunging load when compared with the closed-ended test pile; this is due to the contribution

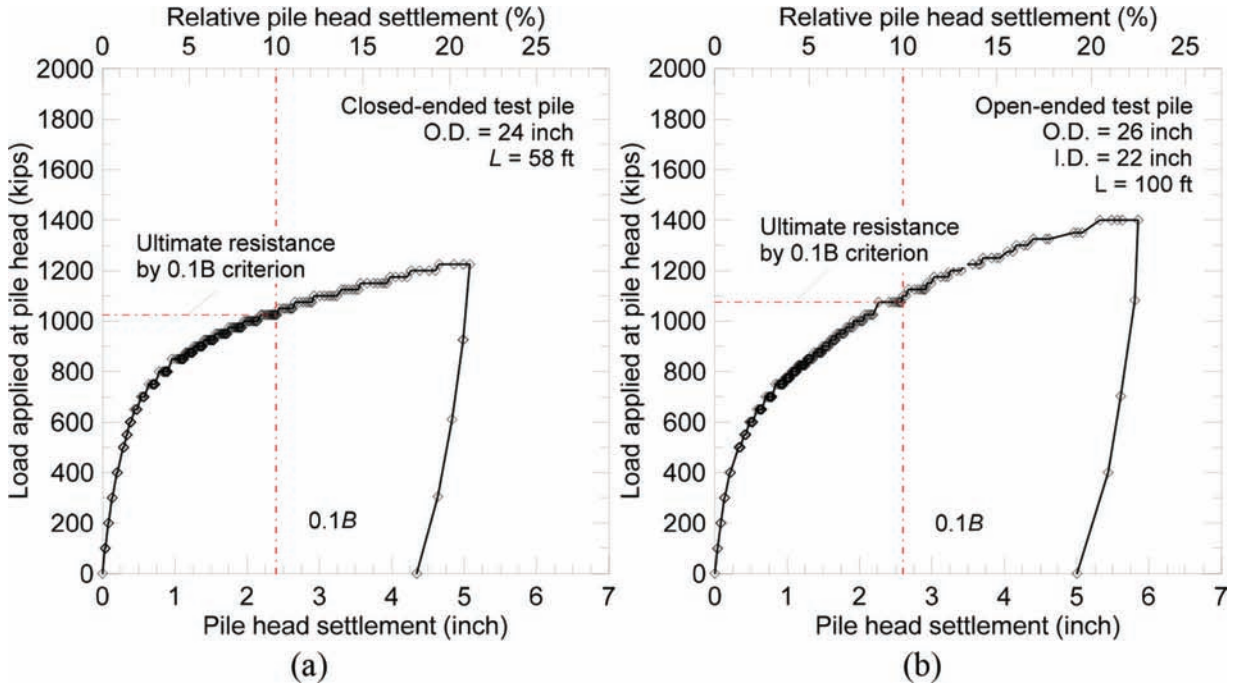

Figure 6.4 Comparison of the load-settlement curves obtained from the static load tests for the (a) closed-ended test pile and (b) open-ended test pile. (Modified after Han, Ganju, Salgado, & Prezzi, in press b.)

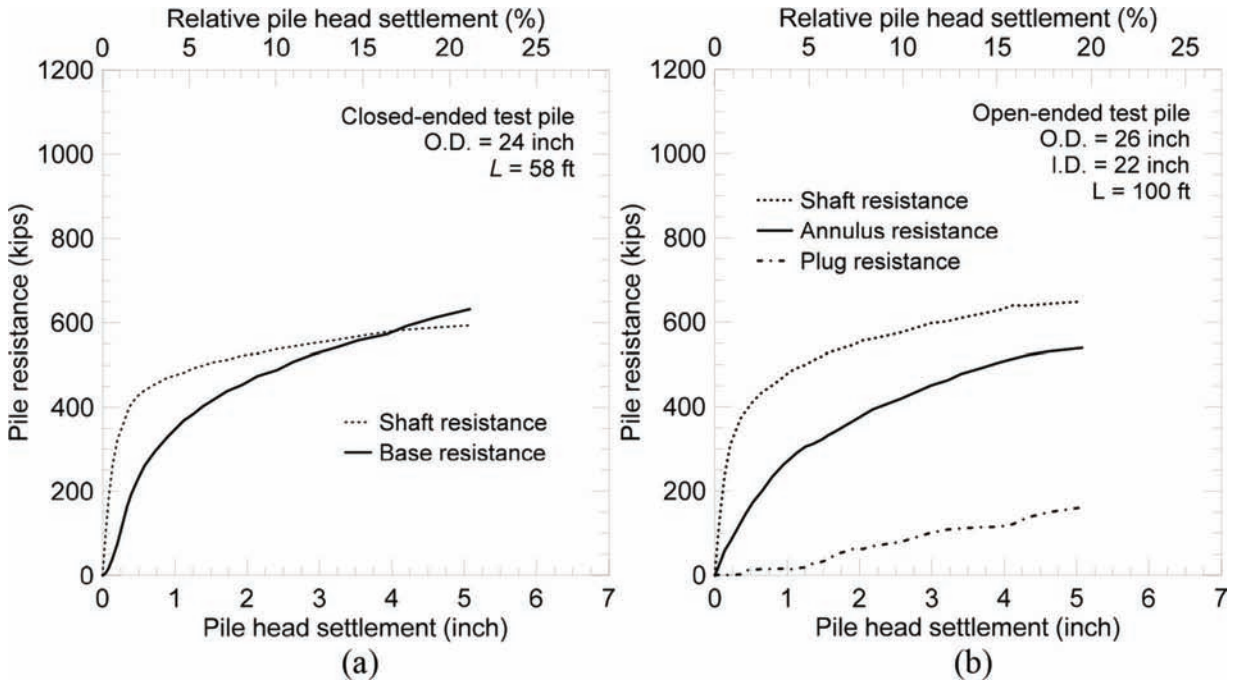

Figure 6.5 Development of the resistance components during the static load tests for the (a) closed-ended test pile and (b) open-ended test pile. (Modified after Han, Ganju, Salgado, & Prezzi, in press b.)

from the plug to the total pile resistance, as explained in the next section.

The total pile resistance measured at the head of a pile is composed of the shaft and base resistances. The shaft resistance mobilized by each soil layer at each loading stage of the pile load tests was directly measured by the strain gauges installed on both the test piles. In the case of the open-ended test pile, which consisted of a double-wall system with outer and inner pipes straining independently, the base resistance was further decomposed into the plug and annulus resistances. Figure 6.5 shows the development of these resistance components as a function of the pile head settlement. The shaft resistances of both test piles were fully

TABLE 6.1
The resistance components measured (at the ultimate load level when $w = 0.1B$) from the static and dynamic load tests

	Test method	Time after initial driving (days)	Shaft resistance (kips)	Plug resistance (kips)	Annulus resistance (kips)	Base resistance[3] (kips)	Total resistance (kips)
Closed-ended test pile	Static load test[1]	13	536	—	—	489	1,025
	Static load test[2]	13	484	—	—	541	1,025
	PDA-EOID[4]	0	211	—	—	280	491
	PDA-BOR[4]	22	263	—	—	275	538
Open-ended test pile	Static load test[1]	8	576	80	419	499	1,075
	Static load test[2]	8	509	70	496	566	1,075
	PDA-EOID[4]	0	328	—	—	175	503
	PDA-BOR[4]	15	236	—	—	305	541

Source: Modified after Han, Ganju, Salgado, & Prezzi, in press b.
[1]Without correction for the residual loads.
[2]After correction for the residual loads.
[3]Equal to the sum of plug and annulus resistances for the open-ended pile.
[4]Obtained from PDA performed by GRL Engineers, Inc.

mobilized at small pile head settlement in the range of 10–20 mm (0.39–0.79 inch). In contrast, the base resistances were mobilized slowly but continuously until the end of the static load tests. The plug resistance, which started to develop only after 30–40 mm (1.18–1.57 inch) of settlement at the head of the open-ended pipe pile, contributed to the additional increase in its total resistance after the ultimate load level had been reached (Figure 6.5). The resistance components obtained from the static and dynamic load tests at the ultimate load level are summarized in Table 6.1. The static capacities estimated from PDAs were conservative when compared with that obtained from the static load test.

6.3 Shaft Resistance

With the readings from the strain gauges densely installed on the test piles, detailed profiles of the unit shaft resistance can be obtained. Figure 6.6 compares the profiles of the unit shaft resistances for the two test piles at the ultimate load level (when $w = 0.1B$). The unit shaft resistance of the closed-ended test pile is significantly greater than that of the open-ended test pile at any depth considered. This is due to the greater level of soil densification and greater lateral stress buildup for the closed-ended test pile than for the open-ended test pile. The open-ended test pile was only partially plugged, with an IFR in the 80%–90% range when at a depth corresponding to the base of the closed-ended test pile.

The unit shaft resistance ratio of the open-ended test pile to the closed-ended test pile is as low as 0.25, which is much lower than the range of 0.5–0.7 as reported in the literature (Paik, Salgado, Lee, & Kim, 2003). This is due to the effect of the shaft degradation caused by pile driving as the two test piles were driven to different depths. A method was proposed by Han, Ganju, Prezzi, and Salgado (in press a) to correct the unit shaft resistance measured from the static load test to the undegraded shaft resistance mobilized before shaft degradation took place. After the correction, the ratio

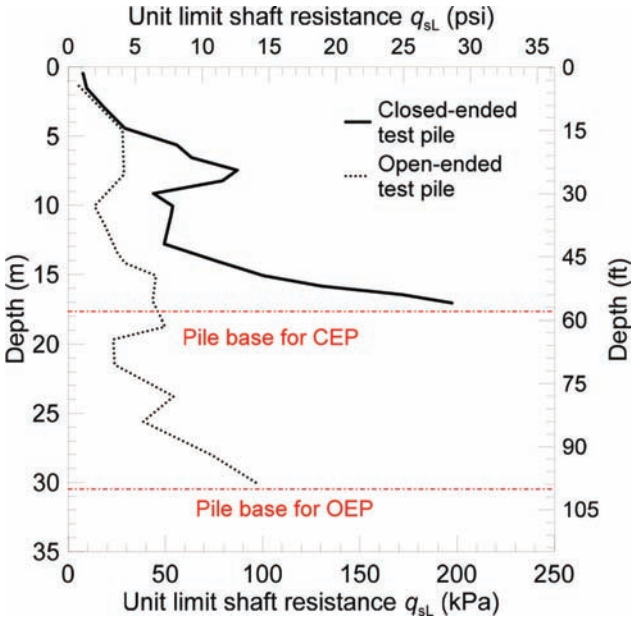

Figure 6.6 Comparison of the unit shaft resistance profiles obtained from the static load tests for the closed-ended and open-ended test piles after correction for the residual loads. (Modified after Han, Ganju, Salgado, & Prezzi, in press b.)

of the undegraded unit shaft resistance for the open-ended test pile to that for the closed-ended test pile lies in the range between 0.4 and 0.8, matching the range reported in the literature.

A number of CPT-based pile design methods have been proposed to estimate the ultimate resistance of closed-ended and open-ended pipe piles driven in sand. The applicability of these design methods for resistance predictions of piles driven in sand containing gravel can be assessed by comparing the resistances measured in the present static load tests with those estimated by using these methods. Figure 6.7 and Figure 6.8 show such a comparison for the closed-ended and open-ended test piles for the Purdue method (Han, Prezzi, Salgado, & Zaheer, 2017), ICP method (Jardine et al., 2005), and

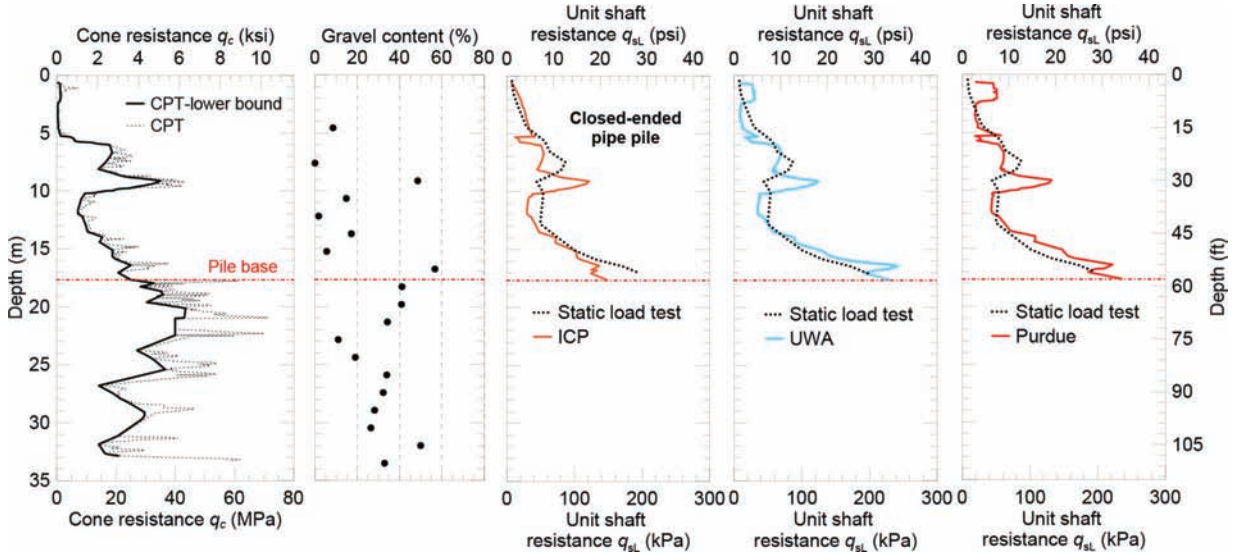

Figure 6.7 Cone resistance q_c, gravel contents, and unit shaft resistance profiles obtained from the static load test and estimated by using CPT-based methods for the closed-ended test pile. (Modified after Han, Ganju, Salgado, & Prezzi, in press b.)

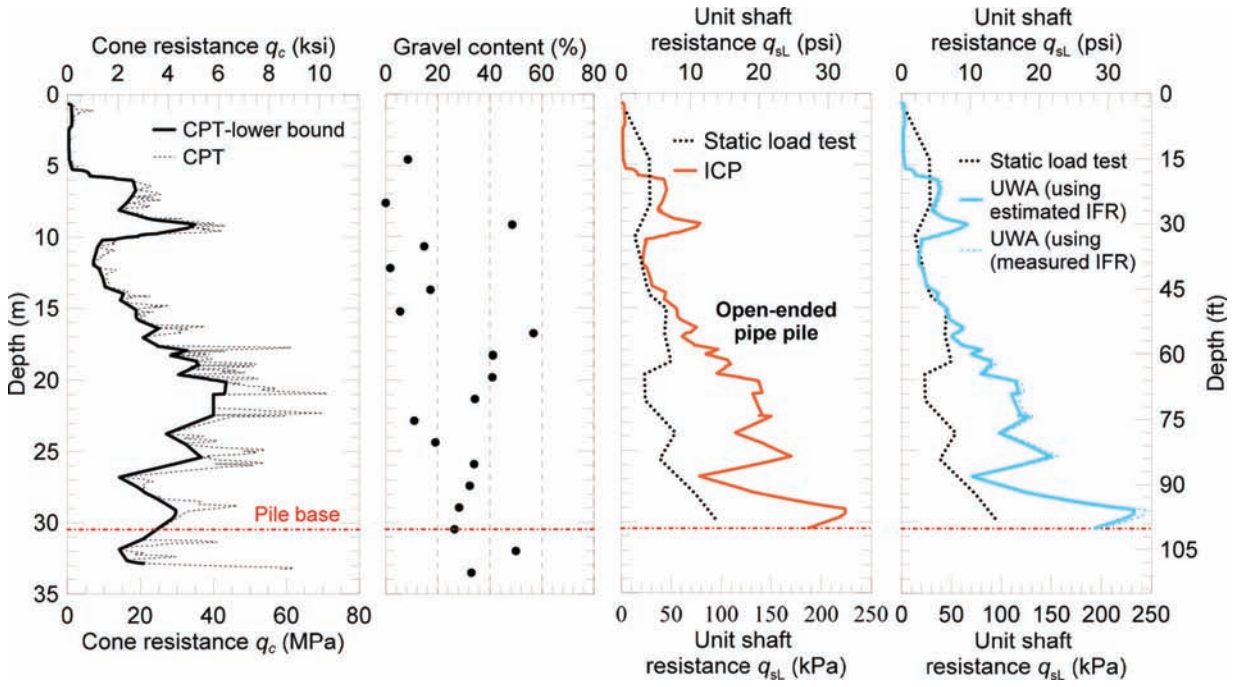

Figure 6.8 Cone resistance q_c, gravel contents, and unit shaft resistance profiles obtained from the static load test and estimated using CPT-based methods for the open-ended test pile. (Modified after Han, Ganju, Salgado, & Prezzi, in press b.)

UWA method (Lehane et al., 2005b). As shown in Figure 6.7, there is good agreement between the predicted and measured unit shaft resistances for the closed-ended pile, except near a depth of about 9 m, where noticeable overprediction is observed. This is because the gravel content of the soil profile was low (<20%) throughout the length of the closed-ended test pile (see Figure 6.7), and therefore the shaft resistance predictions of the CPT-based sand methods were good for most depths. The exception was near $z = 9$ m (29.5 ft), where the gravel content was 49%, resulting in a cone resistance value of almost 40MPa (5802 psi). The existence of large-size particles makes the cone resistance less representative of the soil strength, as the cone may push on a large particle a certain distance in the ground, virtually changing the shape and cross section of the penetrometer. As a result, high cone resistance was measured in sand with high gravel content, leading to overestimation of shaft resistance at that depth.

The effect of the gravel content on cone resistance measurement and the shaft resistance overestimation is also observed for the case of the open-ended test pile.

TABLE 6.2
Unit plug and annulus resistances for the open-ended test pile and base resistance for the closed-ended test pile normalized with respect to the cone resistance at the pile base for different pile head settlement levels

	Open-ended test pile								Closed-ended test pile		
Relative pile head settlement w/B	q_{plug} (MPa)	q_{plug} (psi)	$q_{plug}/q_{cb,avg}$	q_{ann} (MPa)	q_{plug} (psi)	$q_{ann}/q_{cb,avg}$	q_b (MPa)	$q_b/q_{cb,avg}$	q_b (MPa)	q_{plug} (psi)	$q_b/q_{cb,avg}$
0.05	0.2	29	0.01	16.5	2393	0.72	5.09	0.22	6.5	943	0.23
0.1 (ultimate load)	1.3	189	0.06	21.2	3075	0.93	7.21	0.32	8.2	1189	0.29
0.22 (plunging load)	2.8	406	0.12	26.3	3814	1.15	9.78	0.43	10.4	1508	0.36

Source: Modified after Han, Ganju, Salgado, & Prezzi, in press b.
Note: q_{plug} = unit plug resistance; q_{ann} = unit annulus resistance; q_b = unit base resistance.
All the resistances were corrected for the residual loads.

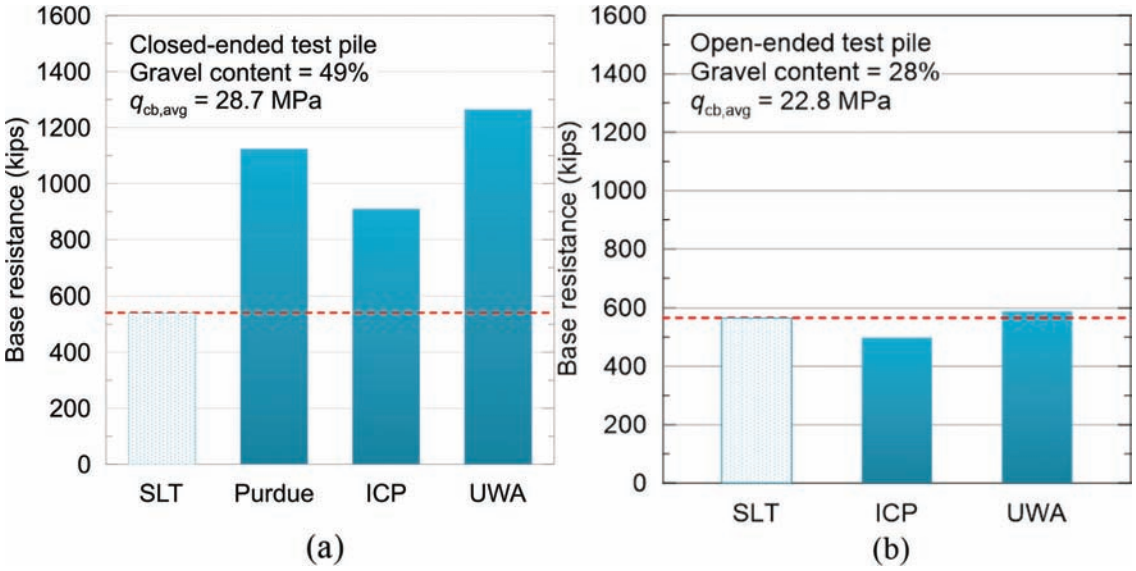

Figure 6.9 Comparison of the base resistances measured from the static load tests with estimations obtained using CPT-based methods for the (a) closed-ended test pile and (b) open-ended test pile. (Modified after Han, Ganju, Salgado, & Prezzi, in press b.)

As shown in Figure 6.8, good agreement between the measured and predicted unit shaft resistances was obtained for most layers above 16 m (52.5 ft), except near 9 m (29.5 ft), and significant overprediction was produced elsewhere. The performance of the CPT-based sand methods is closely related to the gravel content, i.e., overprediction of the unit shaft resistance occurs mostly at depths with large gravel content (50% near z = 9 m (29.5 ft), and mostly in the 30%–40% range at depths greater than 16 m (52.5 ft)).

6.4 Base Resistance

Given the similarities in the mechanisms of mobilization of pile base resistance and cone resistance, the unit base resistance can be directly linked to the cone resistance q_c as a fraction of it (Fleming et al., 2008; Han, Prezzi, Salgado, & Zaheer, 2017; Jardine et al., 2005; Lehane et al., 2005b; Salgado, 2008). Table 6.2 summarizes the unit base resistances (including unit plug and annulus resistances for the open-ended test pile) mobilized at several pile head settlement levels; these resistances are normalized with respect to the average cone resistance at the depth of the corresponding pile base ($q_{cb,avg}$ = 28.7MPa for the closed-ended test pile and $q_{cb,avg}$ = 22.8MPa for the open-ended test pile calculated by averaging q_c from 1B above to 2B below the pile base). Lee et al. (2003) performed open-ended model pile tests in sand, and a q_b/q_c = 0.35 was obtained for the case of IFR = 70% (at the end of pile driving) at the ultimate load level (when w = 0.1B). The value for this ratio is similar to what was obtained in the present pile load test (q_b/q_c = 0.32) at the ultimate load.

The CPT-based pile design methods (Purdue method (Han, Prezzi, Salgado, & Zaheer, 2017), ICP method (Jardine et al., 2005), and UWA method (Lehane et al., 2005b) were used to estimate the ultimate base resistance for the test piles, with the results compared with those obtained from the static load tests in Figure 6.9. Though all three CPT-based methods produced significant overprediction of the base resistance of the closed-ended test pile, they performed well for the open-ended test

pile. The different performances of the design methods for the two test piles is due to the effect of the gravel content and geometry of the pile base. The gravel content was 49% at the base level of the closed-ended test pile, leading to an excessively high q_c value and, thus the overestimation of the base resistance. However, for the open-ended test pile, since the annulus thickness (=51 mm = 2 inch) is similar to the diameter of the CPT cone (B_{CPT} = 44.5 mm = 1.75 inch), the cone resistance is representative of the mobilization of the annulus resistance, which is equal to 87.6% of the base resistance. This makes the CPT-based methods applicable for the prediction of the base resistance of the open-ended test pile, despite the fact that the gravel content at the base level was 28%.

7. SUMMARY AND CONCLUSION

Static and dynamic load tests were performed on large-diameter closed-ended and open-ended pipe piles driven at the construction site for the eastbound Sagamore Parkway Bridge, West Lafayette IN. The test piles were heavily instrumented with both vibrating-wire and electrical-resistance strain gauges at the Bowen Laboratory. A double-wall instrumentation was used for the open-ended test pile to separate measurements for the annulus, inner shaft (plug) and outer shaft resistances. Site investigation consisting of multiple SPTs and CPTs was carried out near the test piles. Soil samples collected from the SPTs were tested in the laboratory to obtain basic soil properties. The soil profile at the construction site consists mainly of sandy soil with various gravel contents at different depths.

Pile driving of the two test piles were monitored. The driving resistance (blow counts) for the closed-ended pile was consistently greater than that of the open-ended pipe at any given depth. The plug formation process (represented by IFR) during installation of the open-ended pile was measured using a weight system. The PLR was 77.7% at the end of driving. Slow-maintained static load tests were performed on the closed-ended and open-ended test piles in tandem. Both test piles were loaded to settlement levels greater than 20% of the pile diameter, when the piles plunged into the ground with a large settlement rate. The data measured from the static load test were processed to generate the load-settlement curves (with each resistance component separated), load transfer curves and unit shaft resistance distributions along the pile length. The residual loads that were locked in the piles after installation were obtained from the electrical-resistance strain gauges.

The resistance components measured from the static load tests were compared with the resistance estimates obtained using CPT-based pile design methods. The design methods provide good estimates for the shaft resistance in sandy soil with low gravel content (<20%) but significantly overpredict the shaft resistance in soil with high gravel content (>30%). Significant overestimation was obtained for the base resistance of the closed-ended pile, because high gravel content (near 50%) was present at the depth of the pile base. Good agreement was found for the base resistances obtained from the design methods and the static load test for the open-ended pile, although the pile base is located in soil with high gravel content. This is because the annulus resistance, which takes the main portion (87.6%) of the base resistance, is well represented by the cone resistance (because of comparable cone diameter with the annulus thickness).

The present study significantly advanced our understanding of the behavior of closed-ended and open-ended pipe piles driven in gravelly sand, and it brought insights to the applicability of the current CPT-based pile design methods for piles in gravelly soil profile. The results obtained from the static pile load tests provide valuable reference for the design of the bridge foundations. The results of this research clearly show that additional research is needed to improve design methods for piles in soil profiles containing gravel.

8. ACKNOWLEDGMENTS

The work presented in this report was funded by the Joint Transportation Research Program (JTRP) administered by the Indiana Department of Transportation (INDOT) and Purdue University through contract SPR-4040. The support of the Indiana Department of Transportation (INDOT) and the Federal Highway Administration (FHWA) and of the JTRP program director, Prof. Darcy Bullock, are gratefully acknowledged. The assistance of the JTRP staff and, in particular, the support received from INDOT technical staff and the Study Advisory Committee members (Mir Zaheer, Youlanda Belew, and Tim Wells) is much appreciated. The authors are also thankful for the continuous support received from the Director of Research & Development, Dr. Barry Partridge and manager of Geotechnical Services, Mr. Athar Khan. The authors acknowledge the help of Kevin Brower, Yohan Casiraghi, Maria Elisa Muller De Faria, Matheus Santanna Andrade, Brunno Godinho Vieira, Shahedur Rahman, Abhishek S.V., and Vibhav Bisht for pile instrumentation and load tests. The authors are also thankful for the support from Jonathan Paauwe from INDOT for site investigation, Jeff Carlson and Patric Tuuk from Superior Construction Company, Inc. for the field operations, and Travis Coleman from GRL Engineers, Inc for providing the PDA data.

REFERENCES

Abu-Farsakh, M. Y., Haque, M. N., & Tsai, C. (2017). A full-scale field study for performance evaluation of axially loaded large-diameter cylinder piles with pipe piles and PSC piles. *Acta Geotechnica*, *12*(4), 753–772. https://doi.org/10.1007/s11440-016-0498-9

Alawneh, A. S., & Malkawi, A. I. H. (2000). Estimation of post-driving residual stresses along driven piles in sand. *ASTM Geotechnical Testing Journal*, *23*(3), 313–326. https://doi.org/10.1520/GTJ11053J

ASTM. (2013). *Standard test method for deep foundations under static axial compressive load* (Report No. D 1143/D 1143M – 07). West Conshohocken, PA: ASTM International. Retrieved from https://compass.astm.org/download/D1143D1143M.26418.pdf

Basu, D., & Salgado, R. (2014). Closure to "Load and Resistance Factor Design of Drilled Shafts in Sand" by D. Basu and Rodrigo Salgado. *Journal of Geotechnical and Geoenvironmental Engineering*, *140*(3), 1455–1469. https://doi.org/10.1061/(ASCE)GT.1943-5606.0001055

Bica, A. V. D., Prezzi, M., Seo, H., Salgado, R., & Kim, D. (2014). Instrumentation and axial load testing of displacement piles. In *Proceedings of the Institution of Civil Engineers - Geotechnical Engineering, 167*(GE3), 238–252. https://doi.org/10.1680/geng.12.00080

Bowman, E. T., & Soga, K. (2005). Mechanisms of setup of displacement piles in sand: Laboratory creep tests. *Canadian Geotechnical Journal*, *42*(5), 1391–1407. https://doi.org/10.1139/t05-063

Briaud, J.–L., Moore, B. H., & Mitchell, G. B. (1989). Analysis of pile load tests at lock and dam 26. In *Foundation engineering: Current principles and practices* (pp. 925–942). New York, NY: American Society of Civil Engineers (ASCE).

Briaud, J.–L., & Tucker, L. (1984). Piles in sand: A method including residual stresses. *Journal of Geotechnical Engineering*, *110*(11), 1666–1680. https://doi.org/10.1061/(ASCE)0733-9410(1984)110:11(1666)

Chow, F. C.–M. (1997). *Investigations into displacement pile behaviour for offshore foundations* (Doctoral thesis, University of London, London, England). Retrieved from Fiona_Ching-Man_Chow-1997-PhD-Thesis.pdf

Clausen, C. J. F., Aas, P. M., & Karlsrud, K. (2005). Bearing capacity of driven piles in sand, the NGI approach. In *Proceedings of International Symposium. on Frontiers in Offshore Geotechnics* (pp. 677–682). London, England: Taylor & Francis.

De Nicola, A., Randolph, M. F. (1993). Tensile and compressive shaft capacity of piles in sand. *Journal of Geotechnical Engineering*, *119*(12), 1952–1973. https://doi.org/10.1061/(ASCE)0733-9410(1993)119:12(1952)

Fellenius, B. H. (2002). Determining the resistance distribution in piles: Part I: Notes on shift of no-load reading and residual load. *Geotechnical News Magazine*, *20*(2), 35–38. Retrieved from https://www.fellenius.net/papers/242%20&%20246%20Load%20Distribution.pdf

Fellenius, B. H., Harris, D. E., & Anderson, D. G. (2004). Static loading test on a 45 m long pipe pile in Sandpoint, Idaho. *Canadian Geotechnical Journal*, *41*(4), 613–628. https://doi.org/10.1139/t04-012

Finlay, T. C. R., White, D. J., Bolton, M. D., & Nagayama, T. (2001). Press-in-piling: The installation of instrumented steel tubular piles with and without driving shoes. In *5th International Conference on Deep Foundations Practice* (pp. 199–208). Hawthorne, NJ: Deep Foundations Institute.

Fleming, K., Weltman, A., Randolph, M., & Elson, K. (2008). *Piling engineering* (3rd ed.). Boca Raton, FL: CRC Press, Taylor & Francis Group.

Foye, K. C., Abou-Jaoude, G. G., Prezzi, M., & Salgado, R. (2009). Resistance factors for use in load and resistance factor design of driven pipe piles in sands. *Journal of Geotechnical and Geoenvironmental Engineering*, *135*(1), 1–13. https://doi.org/10.1061/(ASCE)1090-0241(2009)135:1(1)

Ganju, E., Han, F., Prezzi, M., & Salgado, R. (2019). *Static load test on closed-ended pipe pile driven in gravelly sand.* Manuscript submitted for publication.

Gavin, K., & Lehane, B. (2007). Base load—Displacement response of piles in sand. *Canadian Geotechnical Journal*, *44*(9), 1053–1063. https://doi.org/10.1139/T07-048

Hajduk, E. L., & Paikowsky, S. G. (2000). Performance evaluation of an instrumented test pile cluster. In *Performance Confirmation of Constructed Geotechnical Facilities* (pp. 124–147). Reston, VA: American Society of Civil Engineers (ASCE). https://doi.org/10.1061/40486(300)8

Han, F., Ganju, E., Prezzi, M., Salgado, R., & Zaheer, M. (2019). Axial resistance of open-ended pipe pile driven in gravelly sand. *Géotechnique*. https://doi.org/10.1680/jgeot.18.p.117

Han, F., Ganju, E., Salgado, R., & Prezzi, M. (2018). Effects of interface roughness, particle geometry, and gradation on the sand–steel interface friction angle. *Journal of Geotechnical and Geoenvironmental Engineering*, *144*(12), 04018096-1–04018096-12. https://doi.org/10.1061/(ASCE)GT.1943-5606.0001990

Han, F., Ganju, E., Salgado, R., & Prezzi, M. (in press a). Closure to "Effects of Interface Roughness, Particle Geometry, and Gradation on the Sand–Steel Interface Friction Angle" by Fei Han, Eshan Ganju, Rodrigo Salgado, and Monica Prezzi. *Journal of Geotechnical and Geoenvironmental Engineering*.

Han, F., Ganju, E., Salgado, R., & Prezzi, M. (in press b). Comparison of the load response of closed-ended and open-ended pipe piles driven in gravelly sand. *Acta Geotechnica.*

Han, F., Lim, J., Salgado, R., Prezzi, M., & Zaheer, M. (2015). *Load and resistance factor design of bridge foundations accounting for pile group–soil interaction* (Joint Transportation Research Program Publication No. FHWA/IN/JTRP-2015/24). West Lafayette, IN: Purdue University. https://doi.org/10.5703/1288284316009

Han, F., Prezzi, M., & Salgado, R. (2018). Static and dynamic pile load tests on closed-ended driven pipe pile. In *International Foundations Congress and Equipment Exposition (IFCEE 2018)* (pp. 496–506). Reston, VA: American Society of Civil Engineers (ASCE). https://doi.org/10.1061/9780784481578.047

Han, F., Prezzi, M., Salgado, R., & Zaheer, M. (2017). Axial resistance of closed-ended steel-pipe piles driven in multi-layered soil. *Journal of Geotechnical and Geoenvironmental Engineering*, *143*(3), 04016102-1–04016102-16. https://doi.org/10.1061/%28ASCE%29GT.1943-5606.0001589

Han, F., Salgado, R., & Prezzi, M. (2018). Numerical and experimental study of axially loaded non-displacement piles in sand. In *Proceeding of the 2018 DFI-EFFC International Conference on Deep Foundations and Ground Improvement, Rome, Italy* (pp. 221–229). Hawthorne, NJ: Deep Foundations Institute.

Han, F., Salgado, R., Prezzi, M., & Lim, J. (2017). Shaft and base resistance of non-displacement piles in sand. *Computers and Geotechnics*, *83*, 184–197. https://doi.org/10.1016/j.compgeo.2016.11.006

Igoe, D. J. P., Gavin, K. G., & O'Kelly, B. C. (2011). Shaft capacity of open-ended piles in sand. *Journal of Geotechnical and Geoenvironmental Engineering*, *137*(10), 903–913. https://doi.org/10.1061/(ASCE)GT.1943-5606.0000511

Iskander, M. (2011). On the design of instrumented double-wall model piles used to investigate plugging of open-ended pipe piles. *Geotechnical Testing Journal, 34*(2). 147–154. https://doi.org/10.1520/GTJ103096

Jardine, R., Chow, F., Overy, R., Standing, J., & Jamie, S. (2005). *ICP design methods for driven piles in sands and clays.* London, England: Thomas Telford Ltd.

Jardine, R. J., Lehane, B. M., & Everton, S. J. (1993). Friction coefficients for piles in sands and silts. In *Advances in underwater technology, ocean science and offshore engineering series: Vol 28. Offshore site investigation and foundation behaviour* (pp. 661–677). London, England: Society for Underwater Technology. https://doi.org/10.1007/978-94-017-2473-9_31

Jardine, R. J., Zhu, B. T., Foray, P., & Yang, Z. X. (2013). Measurement of stresses around closed-ended displacement piles in sand. *Géotechnique*, *63*(1), 1–17. https://doi.org/10.1680/geot.9.P.137

Kim, D., Bica, A. V., Salgado, R., Prezzi, M., & Lee, W. (2009). Load testing of a closed-ended pipe pile driven in multilayered soil. *Journal of Geotechnical and Geoenvironmental Engineering*, *135*(4), 463–473. https://doi.org/10.1061/(ASCE)1090-0241(2009)135:4(463)

Kolk, H. J., Baaijens, A. E., & Senders, M. (2005). Design criteria for pipe piles in silica sands. In *Proceedings of International Symposium on Frontiers in Offshore Geotechnics* (pp. 711–716). Boca Raton, FL: CRC Press, Taylor & Francis Group.

Lee, J. H., & Salgado, R. (1999). Determination of pile base resistance in sands. *Journal of Geotechnical and Geoenvironmental Engineering*, *125*(8), 673–683. https://doi.org/10.1061/(ASCE)1090-0241(1999)125:8(673)

Lee, J., Salgado, R., & Paik, K. (2003). Estimation of load capacity of pipe piles in sand based on cone penetration test results. *Journal of Geotechnical and Geoenvironmental Engineering*, *129*(5), 391–403. https://doi.org/10.1061/(ASCE)1090-0241(2003)129:6(391)

Lee, W., Kim, D., Salgado, R., & Zaheer, M. (2010). Setup of driven piles in layered soil. *Soils and Foundations*, *50*(5), 585–598. Retrieved from https://www.jstage.jst.go.jp/article/sandf/50/5/50_5_585/_pdf

Lehane, B. M., & Gavin, K. G. (2001). Base resistance of jacked pipe piles in sand. *Journal of Geotechnical and Geoenvironmental Engineering*, *127*(6), 473–480. https://doi.org/10.1061/(ASCE)1090-0241(2001)127:6(473)

Lehane, B. M., & Randolph, M. F. (2002). Evaluation of a minimum base resistance for driven pipe piles in siliceous sand. *Journal of Geotechnical and Geoenvironmental Engineering*, *128*(3), 198–205. https://doi.org/10.1061/(ASCE)1090-0241(2002)128:3(198)

Lehane, B. M., Schneider, J. A., & Xu, X. (2005a). *A review of design methods for offshore driven piles in siliceous sand*. Perth, Australia: University of Western Australia.

Lehane, B. M., Schneider, J. A., & Xu, X. (2005b). The UWA-05 method for prediction of axial capacity of driven piles in sand. In *Proceedings of the International Symposium on Frontiers in Offshore Geotechnics* (pp. 683–689). Leiden, Netherlands: CRC Press.

Li, Q., Stuedlein, A. W., & Marinucci, A. (2017). Axial load transfer of drilled shaft foundations with and without steel casing. *DFI Journal: The Journal of the Deep Foundations Institute*, *11*(1), 1–17. https://doi.org/10.1080/19375247.2017.1403074

Nevels, J. B., & Snethen, D. R. (1994). Comparison of settlement predictions for single piles in sand based on penetration test results. In *Vertical and horizontal deformations of foundations and embankments* (pp. 1028–1038). Reston, VA: American Society of Civil Engineers (ASCE).

Paik, K., & Salgado, R. (2003). Determination of bearing capacity of open-ended piles in sand. *Journal of Geotechnical and Geoenvironmental Engineering*, *129*(1), 46–57. https://doi.org/10.1061/(ASCE)1090-0241(2003)129:1(46)

Paik, K., Salgado, R., Lee, J., & Kim, B. (2003). Behavior of open- and closed-ended piles driven into sands. *Journal of Geotechnical and Geoenvironmental Engineering*, *129*(4), 296–306. https://doi.org/10.1061/(ASCE)1090-0241(2003)129:4(296)

Paik, K.-H., & Lee, S.–R. (1993). Behavior of soil plugs in open-ended model piles driven into sands. *Marine Georesources & Geotechnology*, *11*(4), 353–373. https://doi.org/10.1080/10641199309379929

Poulos, H. G. (1987). Analysis of residual stress effects in piles. *Journal of Geotechnical Engineering*, *113*(3), 216–229. https://doi.org/10.1061/(ASCE)0733-9410(1987)113:3(216)

Randolph, M. F. (2003). Science and empiricism in pile foundation design. *Géotechnique*, *53*(10), 847–875. https://doi.org/10.1680/geot.2003.53.10.847

Salgado, R. (2008). *The engineering of foundations*. New York City, NY: McGraw-Hills Education.

Salgado, R., Han, F., & Prezzi, M. (2017). Axial resistance of non-displacement piles and pile groups in sand. *Rivista Italiana di Geotecnica*, *51*(4), 35–46.

Salgado, R., Woo, S. I., & Kim, D. (2011). *Development of load and resistance factor design for ultimate and serviceability limit states of transportation structure foundations* (Joint Transportation Research Program Publication No. FHWA/IN/JTRP-2011/03). West Lafayette, IN: Purdue University. https://doi.org/10.5703/1288284314618

Selig, E. (1985). Axial pile loading test—Part 1: Static loading. *Geotechnical Testing Journal*, *8*(2), 79–90. Retrieved from https://doi.org/10.1520/GTJ10514J

Seo, H., Prezzi, M., & Salgado, R. (2013). Instrumented static load test on rock-socketed micropile. *Journal of Geotechnical and Geoenvironmental Engineering*, *139*(12), 2037–2047. https://doi.org/10.1061/(ASCE)GT.1943-5606.0000946

Seo, H., Yildirim, I. Z., & Prezzi, M. (2009). Assessment of the axial load response of an H pile driven in multilayered soil. *Journal of Geotechnical and Geoenvironmental Engineering*, *135*(12), 1789–1804. https://doi.org/10.1061/(ASCE)GT.1943-5606.0000156

Tehrani, F. S., Han, F., Salgado, R., & Prezzi, M. (2017). Laboratory study of the effect of pile surface roughness on the response of soil and non-displacement piles. In *Geotechnical Frontiers 2017* (pp. 256–264). Reston, VA: American Society of Civil Engineers (ASCE). https://doi.org/10.1061/9780784480465.027

Tehrani, F. S., Han, F., Salgado, R., Prezzi, M., Tovar, R. D., & Castro, A. G. (2016). Effect of surface roughness on the shaft resistance of non-displacement piles embedded in sand. *Géotechnique*, *66*(5), 386–400. https://doi.org/10.1680/jgeot.15.P.007

White, D. J., & Bolton, M. D. (2002). Observing friction fatigue on a jacked pile. In *Proceedings of the Workshop on Constitutive and Centrifuge Modelling: Two Extremes* (pp. 346–354). Lisse, Netherlands: CRC Press.

Xu, X., Schneider, J. A., & Lehane, B. M. (2008). Cone penetration test (CPT) methods for end-bearing assessment of open- and closed-ended driven piles in siliceous sand. *Canadian Geotechnical Journal*, *45*(8), 1130–1141. https://doi.org/10.1139/T08-035

About the Joint Transportation Research Program (JTRP)

On March 11, 1937, the Indiana Legislature passed an act which authorized the Indiana State Highway Commission to cooperate with and assist Purdue University in developing the best methods of improving and maintaining the highways of the state and the respective counties thereof. That collaborative effort was called the Joint Highway Research Project (JHRP). In 1997 the collaborative venture was renamed as the Joint Transportation Research Program (JTRP) to reflect the state and national efforts to integrate the management and operation of various transportation modes.

The first studies of JHRP were concerned with Test Road No. 1—evaluation of the weathering characteristics of stabilized materials. After World War II, the JHRP program grew substantially and was regularly producing technical reports. Over 1,600 technical reports are now available, published as part of the JHRP and subsequently JTRP collaborative venture between Purdue University and what is now the Indiana Department of Transportation.

Free online access to all reports is provided through a unique collaboration between JTRP and Purdue Libraries. These are available at http://docs.lib.purdue.edu/jtrp.

Further information about JTRP and its current research program is available at http://www.purdue.edu/jtrp.

About This Report

An open access version of this publication is available online. See the URL in the recommended citation below.

Han, F., Ganju, E., Salgado, R., Prezzi, M., & Zaheer, M. (2019). *Experimental study of the load response of large diameter closed-ended and open-ended pipe piles installed in alluvial soil* (Joint Transportation Research Program Publication No. FHWA/IN/JTRP-2019/03). West Lafayette, IN: Purdue University. https://doi.org/10.5703/1288284316880